

Deformed two center shell model

R. A. Gherghescu^{1,*}

¹ *National Institute of Physics and Nuclear Engineering, RO-76900 Bucharest, Romania*

(Dated: November 9, 2018)

A highly specialized two-center shell model has been developed accounting for the splitting of a deformed parent nucleus into two ellipsoidally deformed fragments. The potential is based on deformed oscillator wells in direct correspondance with the shape change of the nuclear system. For the first time a potential responsible for the necking part between the fragments is introduced on potential theory basis. As a direct consequence, spin-orbit $\mathbf{l}s$ and \mathbf{l}^2 operators are calculated as shape dependent. Level scheme evolution along the fission path for pairs of ellipsoidally deformed fragments is calculated. The Strutinsky method yields the shell corrections for different mass asymmetries from the superheavy nucleus $^{306}_{122}$ and $^{252}_{\text{Cf}}$ all along the splitting process.

INTRODUCTION

From more than thirty years on, two-center shell models are precious tools in the research of fusion, fission and cluster decay processes. The capability of producing transition level schemes during the splitting process from an initial parent nucleus towards two different fragments offers the opportunity of studying what are the possible microscopic changes through a certain fission or decay channel.

In 1961 a symmetric double center oscillator potential has been analyzed by Merzbacher [1]. A strong link was emphasized with regard to diatomic molecules (like ammonia molecule) where the motion in the neighbourhood of an equilibrium state is close to the one generated by a harmonic potential. This problem has been solved for two identical spherical potential wells.

In the 1970's, J. Maruhn, W. Greiner and the Frankfurt school developed the asymmetric two-center shell model [2]. It was an important step for the study of mass asymmetry in binary nuclear fission. The model considered two spherical asymmetric fragments subjected to two-oscillator type potential. A remarkable feature of this model was its ability to describe two overlapping spherical nuclei fission shapes up to their separated configuration. Thus it was possible for microscopic effects to be held responsible as being specifically due to the two emerging and gradually separating level schemes. Basically it is under this form that two center shell models are widely used today in nuclear fusion, fission and cluster decay phenomena.

Two center states in light nuclei are taken into account in connection with molecular orbitals in a two-center shell model picture [3]. Also, application of the two-center shell model on the study of $^{17}\text{O} + ^{12}\text{C}$ reaction has been published [4] with emphasis on nuclear Landau-Zenner effect.

Nucleus-nucleus collisions have also been considered in the framework of the two-center shell model to obtain the two-center level diagrams and single particle corrections for asymmetric systems such as $^{16,17}\text{O} + ^{24,25}\text{Mg}$ [5].

The importance of an adequate description of cold fission, cluster radioactivities and alpha decay in terms of an asymmetric and *deformed* single particle shell model with more realistic shapes during fission and fusion processes was repeatedly stressed [6].

Recently, attempts have been made to use the two-center shell model in synthesis and decay of superheavy nuclei. It is a suitable theoretical model to study the microscopic effects on possible projectile-target combinations in their way from two different quantum systems to one. As the synthesized nucleus is heavier, increasing Coulombian repulsion lowers the macroscopic potential barrier almost to complete disappearance. The only way a superheavy element can survive is due to the shell effects [7]. A two-center shell model is essential for the description of fusion and fission of superheavy elements. It shows that the shell structure of the two participating target-projectile nuclei is visible far beyond the barrier into the fusing nucleus and is crucial in choosing the most favorable pair approaching each other through *cold* fusion valleys. Transition behaviour of the two partner shells will provide shell corrections which lower the fusion barrier to be overcome, as compared to neighbouring projectile-target combinations.

Up to now, all the variants of two-center shell models used spherical nuclei. I shall consider now the motivation of this work. In any process which implies a pass from two quantum systems to one (fusion) or the other way around (fission) there are certain situations when one or both fission fragments or fusion partners are deformed. Such a reaction could yield cold energy valleys due to deformed shell structure of the participants. Fragment deformations are properly accounted in this work. A deformed two-center shell model (DTCSM) is proposed, where the main part of the potential consists of two ellipsoidally deformed Nilsson type oscillators for axially symmetric shapes. Any change in the nuclear surface shape is reflected in a corresponding modification of the four oscillator frequencies along the

symmetry axis and perpendicular to it.

It is also well established that, especially in fission and cluster decay, a necking region builds its way between the fragments, smoothly linking the two ellipsoids one to the other. This work associates for the first time a microscopic potential to a spherically matching neck region of the nuclear shape. The neck potential is constructed in such a way that it takes the same value on the necking region surface as on the ellipsoidal region surfaces of the fragments. Equipotentiality is thus respected on the nuclear surface.

The usual spin-orbit and squared angular momentum operators are calculated with help of the potential-dependent formulae $\mathbf{ls} = (\nabla V \times \mathbf{p})\mathbf{s}$, and $\mathbf{l}^2 = (\nabla V \times \mathbf{p})^2$ [8]. The potential in this model follows exactly the nuclear shape, and so do the \mathbf{ls} and \mathbf{l}^2 operators. Finally, the levels diagram with respect to the elongation, neck parameter and fragment deformations are used to calculate the shell correction by means of the Strutinsky method.

Calculations are presented as an example for different mass asymmetries, for the superheavy nucleus $^{306}122$ and for ^{252}Cf . The dependence on various neck parameter values and on different pairs of fragments is discussed.

SHAPES

Fig. 1 shows the main geometrical parameters defining the axially symmetric shape family DTCSM is dealing with. Two ellipsoids (the deformed fragments) with semiaxes a_1, b_1 and a_2, b_2 are, at a certain moment, separated at a distance R between the two centers O_1 and O_2 . A sphere centered in O_3 with radius R_3 is rolling around the symmetry axis, being tangent all the time to the two ellipsoids. The necking region, between the two tangent points, is generated in this way. Thus we have five independent parameters to design the deformation space: two fragment shape asymmetries $\chi_1 = b_1/a_1$, $\chi_2 = b_2/a_2$ (if a_1 and a_2 are given as the correspondent of β_2 for every A_1 and A_2 , the other semiaxes are calculated from the total volume conservation condition), mass asymmetry A_1/A_2 , the neck radius R_3 and the distance between centers R . Obviously, this set is available for every parent nucleus A, Z with its own $\chi = b/a$.

A few shape sequences obtained by varying two of the parameters, R_3 and R for the same parent and the same mass asymmetry A_1/A_2 are depicted in Fig. 2. Every row starts with the same ellipsoidal parent on the left hand side of the figure. As the distance between centers increases, the two deformed fragments with fixed χ_1 and χ_2 shape asymmetries begin to separate one from the other. Variation with the neck radius R_3 is noticeable on vertical direction. Shape sequences with very small necking region are shown in the upper row (for zero neck radius, $R_3 = 0$ fm, we get compact shapes suitable for fusion reactions), passing through intermediary neck radii, comparable to the magnitude of the ellipsoids semiaxes (second and third row), down to the last row where large neck radius generates very elongated shapes.

This kind of configurations will be microscopically treated along the variation of the deformation space parameters.

THE POTENTIAL

The equations for shape surfaces described in the previous section can be written in cylindrical coordinates (due to axyal symmetry) as:

$$\rho(z) = \begin{cases} \rho_1(z) = [b_1^2 - \chi_1 z^2]^{1/2}, & -a_1 \leq z \leq z_{c1} \\ \rho_g(z) = \rho_3 - [R_3^2 - (z - z_3)^2]^{1/2}, & z_{c1} \leq z \leq z_{c2} \\ \rho_2(z) = [b_2^2 - \chi_2 (z - R)^2]^{1/2}, & z_{c2} \leq z \leq R + a_2 \end{cases} \quad (1)$$

where the origin is placed in the center of the heavy fragment O_1 . Neck sphere center coordinates are (z_3, ρ_3) , and z_{c1} and z_{c2} are the two tangent points of the neck sphere with the two ellipsoids.

The oscillator potential correspondig to these two-center shapes must have the same value on the nuclear surface. For spheres, for example we have:

$$V_0 = \frac{m_0 \omega_i^2 R_i^2}{2} \quad (2)$$

where R_i is the radii of a nucleus with atomic mass A_i . Since $\hbar\omega_i = 41A^{-1/3}$ and $R_i = r_0 A^{1/3}$ (where $r_0 \approx 1.16$) then $V_0 \approx 54.5$ MeV. If we write these simple relations for the surface of ellipsoidal shapes:

$$\begin{aligned}\frac{1}{2}m_0\omega_{z_i}^2 a_i^2 &= V_0 \\ \frac{1}{2}m_0\omega_{\rho_i}^2 b_i^2 &= V_0\end{aligned}\tag{3}$$

the frequencies ω_{z_i} , ω_{ρ_i} are defined along the symmetry axis and respectively perpendicular to it, as functions of the two ellipse semiaxes.

For an arbitrary origin, placed on the symmetry axis, the ellipsoids surface equations read:

$$\begin{aligned}\frac{\rho^2}{\frac{2V_0}{m_0\omega_{\rho_1}^2}} + \frac{(z+z_1)^2}{\frac{2V_0}{m_0\omega_{z_1}^2}} &= 1 \\ \frac{\rho^2}{\frac{2V_0}{m_0\omega_{\rho_2}^2}} + \frac{(z-z_2)^2}{\frac{2V_0}{m_0\omega_{z_2}^2}} &= 1\end{aligned}\tag{4}$$

where z_1 and z_2 are the absolute values of each of the two centers coordinates. Now the two oscillator potential expressions for deformed fragments come straightforward:

$$\begin{aligned}V_1(\rho, z) &= \frac{1}{2}m_0\omega_{\rho_1}^2\rho^2 + \frac{1}{2}m_0\omega_{z_2}^2(z+z_1)^2 \\ V_2(\rho, z) &= \frac{1}{2}m_0\omega_{\rho_2}^2\rho^2 + \frac{1}{2}m_0\omega_{z_2}^2(z-z_2)^2\end{aligned}\tag{5}$$

What we have left to establish is the necking region potential, $V_g(\rho, z)$. The force that keeps nucleons confined within the ellipsoid is an attractive type one, radially inward ($\vec{F}_{ellipsoid} \sim -\vec{r}$). The same reason leads us to the hypothesis that, if nucleons are confined within the concave necking region, which is geometrically *inversed* to the ellipsoid convex surface with respect to the centers of the fragments, a rejective force is needed, radially outward:

$$\vec{F}(\vec{r}) = -\beta\vec{r}\tag{6}$$

hence a force oriented from outside the nuclear shape toward the surface. Then the corresponding potential is related to the expression:

$$\int_0^r \vec{F}d\vec{r} = \varphi(r) - \varphi(0)\tag{7}$$

or

$$\int_0^r \vec{F}d\vec{r} = \int_0^r -\beta\vec{r}d\vec{r} = -\frac{\beta r^2}{2}\tag{8}$$

Consequently, $\varphi(r) = -\frac{\beta r^2}{2}$ is a potential form generating the rejective force. In this way, the rejective neck potential, defined up to a constant, must look like:

$$V_{g1}(r) = V_c + \varphi(r)\tag{9}$$

where V_c is a constant to be determined. On the nuclear surface S_g , we have again:

$$V_{g1} |_{S_g} = V_c + \varphi(r) |_{S_g} = V_0\tag{10}$$

or

$$V_c = V_0 - \varphi(r) |_{S_g} \quad (11)$$

For the sake of consistency, the rejective force is also considered of oscillator type:

$$\vec{F}(\vec{r}) = -m_0\omega_g^2\vec{r} \quad (12)$$

therefore

$$\varphi(r) = -\frac{m_0\omega_g^2 r^2}{2} \quad (13)$$

where the frequency ω_g has to be found. Since the potential must follow the geometrical shape, at the neck region the function $\varphi(r) = \varphi(\rho, z)$ reads:

$$\varphi(\rho, z) = -\frac{m_0\omega_g^2}{2}[(\rho - \rho_3)^2 + (z - z_3)^2] \quad (14)$$

and is centered in the middle of the neck sphere $O_3(\rho_3, z_3)$. On the neck surface then, where $(\rho, z) \in S_g$, we have:

$$\varphi(\rho, z) |_{S_g} = \frac{m_0\omega_g^2}{2}R_3^2 = V_{g1} |_{S_g} = V_0 \quad (15)$$

Then $V_c = V_0 - \varphi(r) |_{S_g} = 2V_0$ and the total neck potential from outside the shape down to the surface is:

$$V_{g1}(r) = 2V_0 - \frac{m_0\omega_g^2}{2}[(\rho - \rho_3)^2 + (z - z_3)^2] \quad (16)$$

and the neck frequency is directly related to the neck radius by Eq. 15. V_{g1} reach its maximum at the center of the neck sphere ($\rho = \rho_3, z = z_3$), where $V_{g1} = 2V_0$, then is decreasing down to the surface value $V_{g1} = V_0$ at a distance equal to the neck radius $(\rho - \rho_3)^2 + (z - z_3)^2 = R_3^2$ from O_3 .

To complete the neck-dependent potential, there still remains the region inside the nuclear shape between the necking surface and the interior contours of the two ellipsoids (black colored, denoted by $V_{g2}(\rho, z)$ in the upper part of Fig. 3). It can be observed that on the ellipsoids surface *inside* the shape the deformed oscillator potential has the same value as on the fragments surface, namely V_0 . But on the surface of the shape within the necking region, the value is also V_0 . Then, one concludes that inside the region volume between the neck surface and the two ellipsoids surfaces - $\rho_1(z) \leq \rho \leq \rho_g(z)$ and $\rho_2(z) \leq \rho \leq \rho_g(z)$ - the neck potential is constant.

$$V_{g2}(\rho, z) = cst = V_0 \quad (17)$$

Finally, the deformed oscillator potential part for the DTCSM reads:

$$V_{DTCSM}(\rho, z) = \begin{cases} V_1(\rho, z) = \frac{1}{2}m_0\omega_{\rho_1}^2\rho^2 + \frac{1}{2}m_0\omega_{z_1}^2(z + z_1)^2 & , v_1 \\ V_g(\rho, z) = \begin{cases} V_{g1}(\rho, z) = 2V_0 - [\frac{1}{2}m_0\omega_g^2(\rho - \rho_3)^2 + \frac{1}{2}m_0\omega_g^2(z - z_3)^2] & , v_{g1} \\ V_{g2}(\rho, z) = V_0 & , v_{g2} \end{cases} \\ V_2(\rho, z) = \frac{1}{2}m_0\omega_{\rho_2}^2\rho^2 + \frac{1}{2}m_0\omega_{z_2}^2(z - z_2)^2 & , v_2 \end{cases} \quad (18)$$

where v_1, v_{g1}, v_{g2} and v_2 are the spatial regions where the corresponding potentials are acting. These regions are about to be revealed further on.

MATCHING POTENTIAL SURFACES

One of the most important issues for the two-center shell models is that the separation plane between the two fragments is not the one where the potentials equal eachother. As an example, for compact shapes (no neck, $R_3 = 0$)

the points ($\{\rho_s, z_s\}$) on the separation line (where the two ellipsae intersect) result in different values for the potentials, $V_1(\rho_s, z_s) \neq V_2(\rho_s, z_s)$. The sharp cusp between the two values makes calculation totally wrong. Attempts to solve the problem by a geometrical transition function, making the frequency $\omega_{\rho_1}(z)$ join $\omega_{\rho_2}(z)$ introduce an unpredictable approximation which is bigger as the mass asymmetry is larger; moreover, it does not reproduce the neck spherical shape and still, only the ρ -part of the potential is solved.

In conclusion, one has to divide the Hilbert space such that the *whole* potential $V_{DTCSM}(\rho, z)$ could smoothly and continuously pass from one fragment to the neck and finally to the other fragment.

First, let us take the deformed fragment oscillators into consideration and find out what are the spatial limits of continuity between the two potentials. The equation for such a region must be complacent with the matching condition:

$$V_1(\rho, z) = V_2(\rho, z) \quad (19)$$

where

$$\begin{aligned} V_1 &= \frac{1}{2}m_0\omega_{\rho_1}^2\rho^2 + \frac{1}{2}m_0\omega_{z_1}^2(z+z_1)^2, S_1(\rho, z) \\ V_2 &= \frac{1}{2}m_0\omega_{\rho_2}^2\rho^2 + \frac{1}{2}m_0\omega_{z_2}^2(z-z_2)^2, S_2(\rho, z) \end{aligned} \quad (20)$$

or

$$\omega_{\rho_1}^2\rho^2 + \omega_{z_1}^2(z+z_1)^2 = \omega_{\rho_2}^2\rho^2 + \omega_{z_2}^2(z-z_2)^2 \quad (21)$$

If one translates the z -coordinate:

$$z = z' - k \quad (22)$$

and separate the terms with respect to the powers of ρ and z' , we get:

$$\begin{aligned} &(\omega_{\rho_1}^2 - \omega_{\rho_2}^2) + (\omega_{z_1}^2 - \omega_{z_2}^2)z'^2 - 2k(\omega_{z_1}^2 - \omega_{z_2}^2)z' + (\omega_{z_1}^2 - \omega_{z_2}^2)k^2 \\ &+ 2(\omega_{z_1}^2 z_1 + \omega_{z_2}^2 z_2)z' - 2(\omega_{z_1}^2 z_1 + \omega_{z_2}^2 z_2)k + \omega_{z_1}^2 z_1^2 - \omega_{z_2}^2 z_2^2 = 0 \end{aligned} \quad (23)$$

We notice that:

$$z_1 + z_2 = R \quad (24)$$

and after some simple calculations one obtains:

$$\frac{\frac{\rho^2}{\omega_{z_1}^2 \omega_{z_2}^2 R^2}}{(\omega_{\rho_2}^2 - \omega_{\rho_1}^2)(\omega_{z_2}^2 - \omega_{z_1}^2)} + \frac{\frac{(z+k)^2}{\omega_{z_1}^2 \omega_{z_2}^2 R^2}}{(\omega_{z_2}^2 - \omega_{z_1}^2)^2} = 1 \quad (25)$$

which defines a so called unique center surface, here namely an ellipsoid with semiaxes:

$$\begin{aligned} a_m &= \frac{\omega_{z_1} \omega_{z_2} R}{\omega_{z_2}^2 - \omega_{z_1}^2} \\ b_m &= \frac{\omega_{z_1} \omega_{z_2} R}{[(\omega_{\rho_2}^2 - \omega_{\rho_1}^2)(\omega_{z_2}^2 - \omega_{z_1}^2)]^{\frac{1}{2}}} \end{aligned} \quad (26)$$

Since the origin of this surface is at ($\rho = 0, z' = 0$), its center with respect to the arbitrary origin (against which the potentials are expressed) is on the symmetry axis at:

$$z_{0m} = k = \frac{a_2^2 z_1 + a_1^2 z_2}{a_1^2 - a_2^2} \quad (27)$$

What we have obtained are the coordinates $(z_{0m}, 0)$ and the semiaxes (a_m, b_m) of a matching potential ellipsoid (MPE). On its surface $V_1(\rho, z) = V_2(\rho, z)$. The heavy deformed fragment O_1 is acting through $V_1(\rho, z)$ outside the MPE. The light fragment part which emerges from the parent is contained inside MPE (the shaded region in Fig. 3). Hence its action on the Hilbert space, $V_2(\rho, z)$, goes all over the matching ellipsoid volume.

The same demonstration is valid for $V_1(\rho, z) = V_{g1}(\rho, z)$, and $V_2(\rho, z) = V_{g2}(\rho, z)$, as far as the neck potential shares its action space with the fragments. First condition:

$$V_1(\rho, z) = V_{g1}(\rho, z) \quad (28)$$

or

$$\frac{1}{2}m_0\omega_{\rho_1}^2\rho^2 + \frac{1}{2}m_0\omega_{z_1}^2(z+z_1)^2 = 2V_0 - [\frac{1}{2}m_0\omega_g^2(\rho-\rho_3)^2 + \frac{1}{2}m_0\omega_g^2(z-z_3)^2] \quad (29)$$

yields:

$$\begin{aligned} & (m_0\omega_{\rho_1}^2 + m_0\omega_g^2)\rho^2 + (m_0\omega_{z_1}^2 + m_0\omega_g^2)z^2 - 2m_0\omega_g^2\rho_3\rho + \\ & 2(m_0\omega_{z_1}^2 z_1 - m_0\omega_g^2 z_3)z + m_0\omega_{z_1}^2 z_1^2 + m_0\omega_g^2(\rho_3^2 + z_3^2) - 4V_0 = 0 \end{aligned} \quad (30)$$

This equation is of the type:

$$a_{11}\rho^2 + a_{22}z^2 + 2a_1\rho + 2a_2z + a = 0 \quad (31)$$

To describe a unique center surface, the normalized determinant of the equation:

$$\frac{\Delta}{\delta} = a - \frac{a_1^2}{a_{11}} - \frac{a_2^2}{a_{22}} \quad (32)$$

must be positive, which is the case for our situation. Then the center of the surface has the coordinates:

$$\rho_{0m1} = \frac{\begin{vmatrix} a_{12} & a_1 \\ a_{22} & a_2 \end{vmatrix}}{\begin{vmatrix} a_{11} & a_{12} \\ a_{21} & a_{22} \end{vmatrix}} \quad z_{0m1} = -\frac{\begin{vmatrix} a_{11} & a_1 \\ a_{21} & a_2 \end{vmatrix}}{\begin{vmatrix} a_{11} & a_{12} \\ a_{21} & a_{22} \end{vmatrix}} \quad (33)$$

After some simple calculations one obtains:

$$\rho_{0m1} = \frac{\omega_g^2 \rho_3}{\omega_{\rho_1}^2 + \omega_g^2} \quad z_{0m1} = \frac{\omega_g^2 z_3 - \omega_{z_1}^2 z_1}{\omega_{z_1}^2 + \omega_g^2} \quad (34)$$

This surface is again an ellipsoid with semiaxes:

$$a_{m1} = \left(-\frac{\Delta}{\delta} \frac{1}{a_{22}} \right)^{1/2} \quad b_{m1} = \left(-\frac{\Delta}{\delta} \frac{1}{a_{11}} \right)^{1/2} \quad (35)$$

and represents the matching potential ellipsoid (MPE1) between $V_1(\rho, z)$ and $V_{g1}(\rho, z)$. On its surface, the two values equal each other. Obviously, the tangent point between this first matching potential ellipsoid and the heavy fragment shape is the same as the tangent point between the neck sphere and the heavy fragment. In the interior of MPE1, the DTCSM potential is $V_{g1}(\rho, z)$. Following the same arguments for:

$$V_2(\rho, z) = V_{g1}(\rho, z) \quad (36)$$

one finds:

$$\rho_{0m2} = \frac{\omega_g^2 \rho_3}{\omega_{\rho_2}^2 + \omega_g^2} \quad z_{0m2} = \frac{\omega_g^2 z_3 - \omega_{z_2}^2 z_2}{\omega_{z_2}^2 + \omega_g^2} \quad (37)$$

for the center of the second neck matching potential ellipsoid (MPE2), and the same expressions with $V_2(\rho, z)$ corresponding values instead of V_1 hold for the semiaxes a_{m2} and b_{m2} .

In the upper part of Fig. 3, the three matching ellipsoids - the large shaded one for $V_1 = V_2$ (MPE) and the two grey ones for $V_1 = V_{g1}$ (MPE1) and $V_2 = V_{g1}$ (MPE2) respectively - are drawn. In this way DTCSM potential spans the whole Hilbert space as follows: within MPE it is $V_2(\rho, z)$ which is active; within the grey area formed by the two neck potential matching ellipsoids, MPE1 and MPE2, we have $V_{g1}(\rho, z)$; in the interior of the nuclear shape, between the neck surface and the fragment ellipsoids surfaces (tiny black region) the potential is $V_{g2}(\rho, z)$. The rest of the space is under $V_1(\rho, z)$ action.

What is achieved in this section is spanning the Hilbert space by DTCSM potential, passing continuously from the potential generated by the heavy fragment V_1 to the lighter one V_2 and allowing also for the neck to be smoothly shaped by V_g . There are no sharp cusps in the potential values. Since we work in axial symmetry, the two neck matching ellipsoids MPE1 and MPE2 are in fact rolling around the symmetry axis. Each of them shapes a thorax around the necking region, where V_{g1} is the DTCSM potential.

On the lower part of Fig. 3 geometrical points which will be used for further calculations are marked: $\rho_{m1s}(z)$ and $\rho_{m1j}(z)$ are MPE1 surface functions, $\rho_{m2s}(z)$ and $\rho_{m2j}(z)$ hold for MPE2, and $\rho_m(z)$ is the surface of MPE. Other points of interest are: z_{c1} and z_{c2} - the two tangent points of the neck *and* MPE1 and MPE2 with the fragment ellipsoids, z_{im} - the intersection of MPE with the symmetry axis, z_{x1l} and z_{x2r} - the left margin of MPE1 and the right margin of MPE2, z_s - the crossing point between the two fragment ellipsoids, z_{mint} - upper crossing point between the three matching ellipsoids

Fig. 4 shows how the three potentials work together. The values of $V_1(\rho, z)$, $V_2(\rho, z)$ and $V_{g1}(\rho, z)$ are taken at $\rho = \rho_1(z_{c1})$ (upper part of the figure), and $\rho = \rho_2(z_{c2})$, hence at the tangent points of the neck sphere. Evolution is shown as the distance R (or z -variable) increases. The values are taken at a matching surface point, thus the potentials are tangent all the time. One can observe how V_1 and V_2 wells are separating with increasing R . The matching surfaces are composed of the whole set of tangent points at every ρ distance from the symmetry axis.

The way two of the potentials, $V_1(\rho, z)$ and $V_{g1}(\rho, z)$, behave along the O_1O_3 line between their two centers is given in Fig. 5. The crossing points of the curves correspond to z_{c1} and its opposite along MPE1. Inside the neck sphere, hence inside MPE1 too, $V_{g1} > V_1$.

DIAGONALIZATION BASIS

This section will browse succinctly the main steps to be taken in order to find a normalized functions set, since details about this issue have already been published [2, 9].

The new feature in the DTCSM eigenvalue problem is the shape-dependency of the potentials: V_{DTCSM} , the spin-orbit term $V_{\Omega s}$ and the V_{Ω^2} term (Ω is preferred here as a notation since the angular momentum operator, as being shape dependent, will be different from the usual \mathbf{l}). The total Hamiltonian:

$$H_{DTCSM} = -\frac{\hbar^2}{2m_0}\Delta + V_{DTCSM}(\rho, z) + V_{\Omega s} + V_{\Omega^2} \quad (38)$$

is obviously not separable. A basis is needed and diagonalization of oscillator potential differences and of angular momentum dependent operators has to be performed.

A separable Hamiltonian is obtained if one takes $\omega_{\rho_1} = \omega_{\rho_2} = \omega_1$, with no $\mathbf{l}s$ and \mathbf{l}^2 terms, hence a potential like:

$$V^{(d)}(\rho, z) = \begin{cases} V_1^{(d)}(\rho, z) = \frac{1}{2}m_0\omega_1^2\rho^2 + \frac{1}{2}m_0\omega_1^2(z + z_1)^2, & z \leq 0 \\ V_2^{(d)}(\rho, z) = \frac{1}{2}m_0\omega_1^2\rho^2 + \frac{1}{2}m_0\omega_2^2(z - z_2)^2, & z \geq 0 \end{cases} \quad (39)$$

This is an appropriate two-center potential for a sphere ($z \leq 0$) intersected with a vertical spheroid. The origin ($z = 0$) is the intersection plane. As a result of variable separation, three known differential equations are obtained for harmonic functions, Laguerre polynomial and Hermite function dependent solutions [9].

Using continuity conditions for z -dependent functions and their derivatives at $z = 0$, the normalization condition and equalizing the energy on the symmetry axis $E_z = \hbar\omega_1(\nu_1 + 0.5) = \hbar\omega_2(\nu_2 + 0.5)$, z -quantum numbers and normalization constants for the z -dependent eigenfunctions are calculated. The ϕ and ρ -dependent functions are straightforward calculated from the differential equations. The final result is:

$$\begin{aligned}\Phi_m(\phi) &= \frac{1}{\sqrt{2\pi}} \exp(im\phi) \\ R_{n_\rho}^{|m|}(\rho) &= \sqrt{\frac{2\Gamma(n_\rho + 1)\alpha_1^2}{\Gamma(n_\rho + |m| + 1)}} \exp\left(-\frac{\alpha_1^2 \rho^2}{2}\right) (\alpha_1^2 \rho^2)^{\frac{|m|}{2}} L_{n_\rho}^{|m|}(\alpha_1^2 \rho^2) \\ Z_\nu(z) &= \begin{cases} C_{\nu_1} \exp\left[-\frac{\alpha_1^2(z+z_1)^2}{2}\right] H_{\nu_1}[-\alpha_1(z+z_1)] & , z < 0 \\ C_{\nu_2} \exp\left[-\frac{\alpha_2^2(z-z_2)^2}{2}\right] H_{\nu_2}[\alpha_2(z-z_2)] & , z \geq 0 \end{cases}\end{aligned}\quad (40)$$

We notice that: where Γ is the gamma function, L_n^m is the m -order Laguerre polynomial, C_1 and C_2 the normalization constants, ν_1, ν_2 the quantum numbers along the symmetry axis, and H_ν is the Hermite function. We now have a basis for further calculations. The eigenvalues for the diagonalized Hamiltonian with the potential $V^{(d)}$ are the oscillator energy levels for sphere+spheroid system:

$$E_{osc}^{(d)} = \hbar\omega_1(2n_\rho + |m| + 1) + \hbar\omega_{z_1}(\nu_1 + 0.5) \quad (41)$$

At this point we have a useful basis for the calculation of H_{DTCSM} matrix elements.

H_{DTCSM} OPERATORS

In order to obtain the DTCSM energy levels, the matrix of the non-diagonal elements should be constructed. Then, adding $E_{osc}^{(d)}$ as diagonal terms, after diagonalization we obtain the eigenvalues.

$V_{DTCSM}(\rho, z)$ - terms

This subsection is devoted to build the operators for the necked-in deformed two-center oscillator levels calculation. We start with the operators leading to the appropriate energies for $V_1(\rho, z)$. The difference $V_1(\rho, z) - V^{(d)}(\rho, z)$ on the volume v_1 and added to $E^{(d)}(n_\rho, \nu, m)$ produce the suitable matrix elements for V_1 :

$$\begin{aligned}\Delta V_1 &= \Delta V_1(-\infty, z_{im}) + \Delta V_1(z_{im}, 0) + \Delta V_1(0, z_{0m} + a_m) + \Delta V_1(z_{0m} + a_m, \infty) \\ &\quad - \Delta V_1(z_{x1l} \div z_{c1}; \rho_{m1j} \div \rho_{m1s}) - \Delta V_1(z_{c1} \div z_s; \rho_1 \div \rho_{m1s}) - \Delta V_1(z_s \div z_{mint}; \rho_m \div \rho_{m1s})\end{aligned}\quad (42)$$

The positive terms account for the influence of $V_1(\rho, z)$ as if V_1 would act alone everywhere but MPE. The negative terms are under $V_g(\rho, z)$ action. In parenthesis are the geometrical limits for every term. Note that for those which have also ρ -dependent limits, $\rho = \rho(z)$. The limits can be easily tracked in Fig. 3. What is left after the subtraction is the difference from $V_1(\rho, z)$ to $V^{(d)}(\rho, z)$ within the v_1 volume. To ease calculations, one uses as a notation:

$$\Delta V_1^{(p)} = \Delta V_1(-\infty, z_{im}) + \Delta V_1(z_{im}, 0) + \Delta V_1(0, z_{0m} + a_m) + \Delta V_1(z_{0m} + a_m, \infty) \quad (43)$$

These positive potential differences are now written in terms of the Heavyside step function; this will result in determining the exact limits where $V_1(\rho, z)$ is acting and, consequently, where it decides the oscillator energy values :

$$\begin{aligned}\Delta V_1^{(p)} &= \frac{1}{2}(m_0\omega_{\rho_1}^2 - m_0\omega_1^2)\{[1 - \theta(z - z_{im})] + \theta[z - (z_{0m} + a_m)]\}\rho^2 \\ &\quad + \frac{1}{2}\{(m_0\omega_{z_1}^2 - m_0\omega_1^2)(z + z_1)^2[1 - \theta(z - z_{im})] \\ &\quad + [m_0\omega_{z_1}^2(z + z_1)^2 - m_0\omega_2^2(z - z_2)^2]\theta[z - (z_{0m} + a_m)]\}\delta_{n_\rho, n_\rho}\end{aligned}\quad (44)$$

$$\begin{aligned}
& + \frac{1}{2}(m_0\omega_{\rho_1}^2 - m_0\omega_1^2)\{\theta(z - z_{im}) - \theta(z)\} \\
& + [\theta(z) - \theta[z - (z_{0m} + a_m)]]\rho^2\theta(\rho - \rho_m(z)) \\
& + \frac{1}{2}\{(m_0\omega_{z_1}^2 - m_0\omega_1^2)(z + z_1)^2[\theta(z - z_{im}) - \theta(z)] \\
& + [m_0\omega_{z_1}^2(z + z_1)^2 - m_0\omega_2^2(z - z_2)^2][\theta(z) - \theta[z - (z_{0m} + a_m)]]\}\theta(\rho - \rho_m(z))
\end{aligned}$$

For the negative differences we have:

$$\begin{aligned}
\Delta V_1(z_i \div z_f; \rho_i(z) \div \rho_f(z)) = \\
\frac{1}{2}m_0\omega_{\rho_1}^2[\theta(z - z_i)\theta(z - z_f)]\rho^2[\theta(\rho - \rho_i(z)) - \theta(\rho - \rho_f(z))] \\
+ \frac{1}{2}m_0\omega_{z_1}^2(z + z_1)^2[\theta(z - z_i) - \theta(z - z_f)][\theta(\rho - \rho_i(z)) - \theta(\rho - \rho_f(z))]
\end{aligned} \tag{45}$$

where z_i , z_f , $\rho_i(z)$ and $\rho_f(z)$ take the corresponding values and limit functions from Eq. 45.

To obtain the terms where the light emerged fragment potential $V_2(\rho, z)$ acts, one must subtract $V^{(d)}(\rho, z)$ from $V_2(\rho, z)$ within the v_2 volume. The result is:

$$\begin{aligned}
\Delta V_2 = \\
\Delta V_2(z_{im} \div 0; 0 \div \rho_m(z)) + \Delta V_2(0 \div z_{0m} + a_m; 0 \div \rho_m(z)) \\
- \Delta V_2(z_s \div z_{c2}; \rho_g(z) \div \rho_m(z)) - \Delta V_2(z_{mint} \div z_{x2r}; \rho_{m2j}(z) \div \rho_{m2s}(z))
\end{aligned} \tag{46}$$

Let us denote:

$$\Delta V_2^{(p)} = \Delta V_2(z_{im} \div 0; 0 \div \rho_m(z)) + \Delta V_2(0 \div z_{0m} + a_m; 0 \div \rho_m(z)) \tag{47}$$

Then we have:

$$\begin{aligned}
\Delta V_2^{(p)} = \\
\frac{1}{2}(m_0\omega_{\rho_2}^2 - m_0\omega_1^2)\{\theta[z - (z_{0m} + a_m)]\}\rho^2[1 - \theta(\rho - \rho_m(z))] \\
+ \frac{1}{2}\{[m_0\omega_{z_2}^2(z - z_2)^2 - m_0\omega_1^2(z + z_1)^2][\theta(z - z_{im}) - \theta(z)] \\
+ (m_0\omega_{z_2}^2 - m_0\omega_2^2)(z - z_2)^2\{\theta(z) - \theta[z - (z_{0m} + a_m)]\}\}[1 - \theta(\rho - \rho_m(z))]
\end{aligned} \tag{48}$$

for the positive part; for the negative necking region which has to be subtracted from v_2 , the expression for any $\Delta V_2(z_i \div z_f; \rho_i(z) \div \rho_f(z))$ is:

$$\Delta V_2(z_i \div z_f; \rho_i(z) \div \rho_f(z)) = \tag{49}$$

$$\begin{aligned}
& \frac{1}{2}m_0\omega_{\rho_2}^2[\theta(z - z_i) - \theta(z - z_f)]\rho^2[\theta(\rho - \rho_i(z)) - \theta(\rho - \rho_f(z))] \\
& + \frac{1}{2}m_0\omega_{z_2}^2(z - z_2)^2[\theta(z - z_i) - \theta(z - z_f)][\theta(\rho - \rho_i(z)) - \theta(\rho - \rho_f(z))]
\end{aligned} \tag{50}$$

using the same convention for z_i , z_f , ρ_i and $\rho_f(z)$ as for ΔV_1 .

At this point, the neck potential $V_g(\rho, z)$ is filling its volume v_g without any subtraction:

$$\Delta V_g = V_g \tag{51}$$

With the same notation as in Eq. 18 we have for the neck operators:

$$V_g = V_{g1}(v_{g1}) + V_{g2}(v_{g2}) \quad (52)$$

Now every of them will be taken separately:

$$V_{g1} = V_{g1}(z_{x1l} \div z_{c1}; \rho_{m1j} \div \rho_{m1s}) + V_{g1}(z_{c1} \div z_{mint}; \rho_g \div \rho_{m1s}) + V_{g1}(z_{mint} \div z_{x2r}; \rho_{m2j} \div \rho_{m2s}) \quad (53)$$

$$V_{g2} = V_{g2}(z_{c1} \div z_s; \rho_1(z) \div \rho_g(z)) + V_{g2}(z_s \div z_{c2}; \rho_2(z) \div \rho_g(z)) \quad (54)$$

where again:

$$\begin{aligned} V_{g1}(z_i \div z_f; \rho_i \div \rho_f) = & \\ & 2V_0[\theta(z - z_i) - \theta(z - z_f)][\theta(\rho - \rho_i(z)) - \theta(\rho - \rho_f(z))] \\ & - \frac{1}{2}m_0\omega_g^2[\theta(z - z_i) - \theta(z - z_f)](\rho - \rho_3)^2[\theta(\rho - \rho_i(z)) - \theta(\rho - \rho_f(z))] \\ & - \frac{1}{2}m_0\omega_g^2(z - z_3)^2[\theta(z - z_i) - \theta(z - z_f)][\theta(\rho - \rho_i(z)) - \theta(\rho - \rho_f(z))] \end{aligned} \quad (55)$$

and

$$V_{g2}(z_i \div z_f; \rho_i \div \rho_f) = V_0\{[\theta(z - z_i) - \theta(z - z_f)][\theta(\rho - \rho_i(z)) - \theta(\rho - \rho_f(z))]\} \quad (56)$$

The final analytical expressions for the matrix elements corresponding to the oscillator potential of DTCSM are given in Appendix A.

Spin-orbit \mathbf{l}_s and \mathbf{l}^2 operators

Special care will be devoted to the treatment of $V_{\mathbf{l}_s}$ and $V_{\mathbf{l}^2}$ matrix elements. Because of the dependence of the angular momentum term on different space regions ($\sim \nabla V \times \mathbf{p}$), hence on different mass regions when asymmetry A_1/A_2 comes in, the anticommutator is used to assure hermicity for the operators:

$$V_{\mathbf{l}_s} = \begin{cases} -\left\{ \frac{\hbar}{m_0\omega_{01}} \kappa_1(\rho, z), (\nabla V \times \mathbf{p})\mathbf{s} \right\}, & A_1 - region \\ -\left\{ \frac{\hbar}{m_0\omega_{02}} \kappa_2(\rho, z), (\nabla V \times \mathbf{p})\mathbf{s} \right\}, & A_2 - region \end{cases} \quad (57)$$

and

$$V_{\mathbf{l}^2} = \begin{cases} -\left\{ \frac{\hbar}{m_0^2\omega_{01}^3} \kappa_1\mu_1(\rho, z), (\nabla V \times \mathbf{p})^2 \right\}, & A_1 - region \\ -\left\{ \frac{\hbar}{m_0^2\omega_{02}^3} \kappa_2\mu_2(\rho, z), (\nabla V \times \mathbf{p})^2 \right\}, & A_2 - region \end{cases} \quad (58)$$

Basically the same treatment as for oscillator terms is valid in this case. The $\kappa_1(\rho, z)$ and $\mu_1(\rho, z)$ are the strength function parameters for the $V_1(\rho, z)$ region, whereas $\kappa_2(\rho, z)$ and $\mu_2(\rho, z)$ are active for the $V_2(\rho, z)$ one.

The new feature here is the use of the anticommutator for the operators containing Heavyside function combinations, to confine the action to v_1 , v_2 and v_g ; these function combinations are exactly the ones which have been used for ΔV_1 , ΔV_2 and ΔV_g terms.

Since the creation and anihilation angular momentum operators become shape-frequency dependent, notations will be changed as follows:

$$\mathbf{l}^+ \rightarrow \boldsymbol{\Omega}^+ \quad \mathbf{l}^- \rightarrow \boldsymbol{\Omega}^- \quad \mathbf{l}_z \rightarrow \boldsymbol{\Omega}_z$$

so that

$$\mathbf{l}\mathbf{s} \rightarrow \frac{1}{2}(\boldsymbol{\Omega}^+\mathbf{s}^- + \boldsymbol{\Omega}^-\mathbf{s}^+) + \boldsymbol{\Omega}_z\mathbf{s}_z \quad (59)$$

Then for the potentials of the spin-orbit term to be diagonalized one reads:

$$V_{\boldsymbol{\Omega}\mathbf{s}} = V_{\boldsymbol{\Omega}\mathbf{s}}(v_1) + V_{\boldsymbol{\Omega}\mathbf{s}}(v_2) + V_{\boldsymbol{\Omega}\mathbf{s}}(v_g) \quad (60)$$

where:

$$V_{\boldsymbol{\Omega}\mathbf{s}}(v_1) = -\frac{\hbar}{m_0\omega_{01}}\kappa_1\{\boldsymbol{\Omega}\mathbf{s}, (v_1)\} \quad (61)$$

$$V_{\boldsymbol{\Omega}\mathbf{s}}(v_2) = -\frac{\hbar}{m_0\omega_{02}}\kappa_2\{\boldsymbol{\Omega}\mathbf{s}, (v_2)\} \quad (62)$$

$$V_{\boldsymbol{\Omega}\mathbf{s}}(v_g) = -\frac{\hbar}{m_0\omega_{01}}\kappa_1\{\boldsymbol{\Omega}\mathbf{s}, (v_g^{(1)})\} - \frac{\hbar}{m_0\omega_{02}}\kappa_2\{\boldsymbol{\Omega}\mathbf{s}, (v_g^{(2)})\} \quad (63)$$

where $v_g^{(1)}$ and $v_g^{(2)}$ are the neck matching ellipsoids volumes on A_1 and A_2 side, respectively.

On the other hand, the operators depend on the region they exert themselves through the potentials, according to Eq. 57. Thus we have:

$$\begin{aligned} \boldsymbol{\Omega}^+(v_1) &= -e^{i\varphi} \left[\frac{\partial V_1(\rho, z)}{\partial \rho} \frac{\partial}{\partial z} - \frac{\partial V_1(\rho, z)}{\partial z} \frac{\partial}{\partial \rho} - \frac{i}{\rho} \frac{\partial V_1(\rho, z)}{\partial z} \frac{\partial}{\partial \varphi} \right] \\ &= -e^{i\varphi} \left[m_0\omega_{\rho_1}^2 \rho \frac{\partial}{\partial z} - m_0\omega_{z_1}^2 (z + z_1) \frac{\partial}{\partial \rho} - \frac{i}{\rho} m_0\omega_{z_1}^2 (z + z_1) \frac{\partial}{\partial \varphi} \right] \end{aligned} \quad (64)$$

$$\begin{aligned} \boldsymbol{\Omega}^-(v_1) &= e^{-i\varphi} \left[\frac{\partial V_1(\rho, z)}{\partial \rho} \frac{\partial}{\partial z} - \frac{\partial V_1(\rho, z)}{\partial z} \frac{\partial}{\partial \rho} + \frac{i}{\rho} \frac{\partial V_1(\rho, z)}{\partial z} \frac{\partial}{\partial \varphi} \right] \\ &= e^{-i\varphi} \left[m_0\omega_{\rho_1}^2 \rho \frac{\partial}{\partial z} - m_0\omega_{z_1}^2 (z + z_1) \frac{\partial}{\partial \rho} + \frac{i}{\rho} m_0\omega_{z_1}^2 (z + z_1) \frac{\partial}{\partial \varphi} \right] \end{aligned} \quad (65)$$

$$\begin{aligned} \boldsymbol{\Omega}_z(v_1) &= -\frac{i}{\rho} \frac{\partial V_1}{\partial \rho} \frac{\partial}{\partial \varphi} \\ &= -im_0\omega_{\rho_1}^2 \frac{\partial}{\partial \varphi} \end{aligned} \quad (66)$$

with

$$\boldsymbol{\Omega}\mathbf{s}(v_1) = \frac{1}{2}(\boldsymbol{\Omega}^+(v_1)\mathbf{s}^- + \boldsymbol{\Omega}^-\mathbf{s}^+) + \boldsymbol{\Omega}_z(v_1)\mathbf{s}_z \quad (67)$$

The same applies for (v_2) and (v_g) spin-orbit operators terms, and the expressions are:

$$\begin{aligned}
\Omega^+(v_2) &= -e^{i\varphi} \left[m_0\omega_{\rho_2}^2 \rho \frac{\partial}{\partial z} - m_0\omega_{z_2}^2 (z - z_2) \frac{\partial}{\partial \rho} - \frac{i}{\rho} m_0\omega_{z_2}^2 (z - z_2) \frac{\partial}{\partial \varphi} \right] \\
\Omega^-(v_2) &= e^{-i\varphi} \left[m_0\omega_{\rho_2}^2 \rho \frac{\partial}{\partial z} - m_0\omega_{z_2}^2 (z - z_2) \frac{\partial}{\partial \rho} + \frac{i}{\rho} m_0\omega_{z_2}^2 (z - z_2) \frac{\partial}{\partial \varphi} \right] \\
\Omega_z(v_2) &= -im_0\omega_{\rho_2}^2 \frac{\partial}{\partial \varphi}
\end{aligned} \tag{68}$$

and:

$$\begin{aligned}
\Omega^+(v_{g1}) &= -e^{i\varphi} \left[m_0\omega_g^2 (\rho - \rho_3) \frac{\partial}{\partial z} - m_0\omega_g^2 (z - z_3) \frac{\partial}{\partial \rho} - \frac{i}{\rho} m_0\omega_g^2 (z - z_3) \frac{\partial}{\partial \varphi} \right] \\
\Omega^-(v_{g1}) &= e^{-i\varphi} \left[m_0\omega_g^2 (\rho - \rho_3) \frac{\partial}{\partial z} - m_0\omega_g^2 (z - z_3) \frac{\partial}{\partial \rho} + \frac{i}{\rho} m_0\omega_g^2 (z - z_3) \frac{\partial}{\partial \varphi} \right] \\
\Omega_z(v_{g1}) &= im_0\omega_g^2 \frac{\rho - \rho_3}{\rho} \frac{\partial}{\partial \varphi}
\end{aligned} \tag{69}$$

and $\Omega_s(v_{g2}) = 0$, since $V_g(v_{g2}) = V_0 = cst$. With the help of these operators, what is to be calculated now for the spin-orbit shape-dependent matrix elements reads, for (v_1) :

$$V_{\Omega s}(v_1) = -\frac{\hbar}{m_0\omega_{01}} \kappa_1 \{ \Omega s(v_1), (v_1) \} \tag{70}$$

where:

$$\begin{aligned}
\{ \Omega s(v_1), (v_1) \} = & \\
& \{ \Omega s(v_1), [1 - \theta(z - z_{im})] \} + \{ \Omega s(v_1), \theta[z - (z_{0m} + a_m)] \} \\
& + \{ \Omega s(v_1), [\theta(z - z_{im}) - \theta[z - (z_{0m} + a_m)]] \theta(\rho - \rho_m(z)) \} \\
& - \{ \Omega s(v_1), [\theta(z - z_{x1l}) - \theta(z - z_{c1})] [\theta(\rho - \rho_{m1j}(z)) - \theta(\rho - \rho_{m1s}(z))] \} \\
& - \{ \Omega s(v_1), [\theta(z - z_{c1}) - \theta(z - z_s)] [\theta(\rho - \rho_1(z)) - \theta(\rho - \rho_{m1s}(z))] \} \\
& - \{ \Omega s(v_1), [\theta(z - z_s) - \theta(z - z_{mint})] [\theta(\rho - \rho_m(z)) - \theta(\rho - \rho_{m1s}(z))] \}
\end{aligned} \tag{71}$$

For the $V_2(\rho, z)$ controlled region we have:

$$V_{\Omega s}(v_2) = -\frac{\hbar}{m_0\omega_{02}} \kappa_2 \{ \Omega s(v_2), (v_2) \} \tag{72}$$

where:

$$\begin{aligned}
\{ \Omega s(v_2), (v_2) \} = & \\
& \{ \Omega s(v_2), [\theta(z - z_{im}) - \theta[z - (z_{0m} + a_m)]] [1 - \theta(\rho - \rho_m(z))] \} \\
& - \{ \Omega s(v_2), [\theta(z - z_s) - \theta(z - z_{c2})] [\theta(\rho - \rho_2(z)) - \theta(\rho - \rho_g(z))] \} \\
& - \{ \Omega s(v_2), [\theta(z - z_{gm}) - \theta(z - z_{mint})] [\theta(\rho - \rho_g(z)) - \theta(\rho - \rho_m(z))] \} \\
& - \{ \Omega s(v_2), [\theta(z - z_{mint}) - \theta(z - z_{x2r})] [\theta(\rho - \rho_{m2j}(z)) - \theta(\rho - \rho_{m2s}(z))] \}
\end{aligned} \tag{73}$$

Finally, the neck potential dependent spin-orbit interaction looks like:

$$V_{\Omega s}(v_g) = -\frac{\hbar}{m_0\omega_{01}} \kappa_1 \{ \Omega s(v_{g1}), (v_{g1}^{(1)}) \} - \frac{\hbar}{m_0\omega_{02}} \kappa_2 \{ \Omega s(v_{g1}), (v_{g1}^{(2)}) \} \tag{74}$$

where:

$$\begin{aligned} \{\mathbf{\Omega s}(v_{g1}), (v_{g1}^{(1)})\} = \\ \{\mathbf{\Omega s}(v_{g1}), [\theta(z - z_{x1l}) - \theta(z - z_{c1})][\theta(\rho - \rho_{m1j}(z)) - \theta(\rho - \rho_{m1s}(z))]\} \\ + \{\mathbf{\Omega s}(v_{g1}), [\theta(z - z_{c1}) - \theta(z - z_{mint})][\theta(\rho - \rho_g(z)) - \theta(\rho - \rho_{m1s}(z))]\} \end{aligned} \quad (75)$$

$$\begin{aligned} \{\mathbf{\Omega s}(v_{g1}), (v_{g1}^{(2)})\} = \\ \{\mathbf{\Omega s}(v_{g1}), [\theta(z - z_{mint}) - \theta(z - z_{x2r})][\theta(\rho - \rho_{m2j}(z)) - \theta(\rho - \rho_{m2s}(z))]\} \end{aligned} \quad (76)$$

For the $\mathbf{I}^2 \rightarrow \mathbf{\Omega}^2$ term the usual expression works:

$$\mathbf{\Omega}^2 = \frac{1}{2}(\mathbf{\Omega}^+ \mathbf{\Omega}^- + \mathbf{\Omega}^- \mathbf{\Omega}^+) + \mathbf{\Omega}_z^2 \quad (77)$$

and the operator for the whole space is:

$$V_{\mathbf{\Omega}^2} = -\frac{1}{2} \left\{ \frac{\hbar}{m_0^2 \omega_{0i}^3} \kappa_i \mu_i(\rho, z), \mathbf{\Omega}^2 \right\}, \quad i = 1, 2 \quad (78)$$

Strength coefficients $\kappa_1 \mu_1(\rho, z)$ and $\kappa_2 \mu_2(\rho, z)$ are the same (ρ, z) - dependent functions as $\kappa_1(\rho, z)$ and $\kappa_2(\rho, z)$ in the spin-orbit term. Making use of the unity operator $I = \sum_{''} |''\rangle \langle ''|$, many expressions can be derived to obtain an easy workable decomposition of the lengthy matrix elements of $V_{\mathbf{\Omega}^2}$. The chosen one follows, in order to make use of the already calculated expression for $\mathbf{\Omega s}$ term:

$$\begin{aligned} \langle' | \{f(\rho, z), \mathbf{\Omega}^+ \mathbf{\Omega}^-\} | \rangle = \\ \sum_{''} [2 \langle' | \{f(\rho, z), \mathbf{\Omega}^+\} | ''\rangle + \langle' | (\mathbf{\Omega}^+ f(\rho, z)) | ''\rangle \langle '' | \mathbf{\Omega}^- | \rangle + \langle' | \mathbf{\Omega}^+ | ''\rangle \langle '' | (\mathbf{\Omega}^- f(\rho, z)) | \rangle] \end{aligned} \quad (79)$$

$$\begin{aligned} \langle' | \{f(\rho, z), \mathbf{\Omega}^- \mathbf{\Omega}^+\} | \rangle = \\ \sum_{''} [2 \langle' | \{f(\rho, z), \mathbf{\Omega}^-\} | ''\rangle + \langle' | (\mathbf{\Omega}^- f(\rho, z)) | ''\rangle \langle '' | \mathbf{\Omega}^+ | \rangle + \langle' | \mathbf{\Omega}^- | ''\rangle \langle '' | (\mathbf{\Omega}^+ f(\rho, z)) | \rangle] \end{aligned} \quad (80)$$

The needed expressions for the $\mathbf{\Omega s}$ and $\mathbf{\Omega}^2$ matrix elements are detailed in Appendix B.

Now the total matrix elements for DTCSM can be calculated as:

$$\langle i | DTCSM | j \rangle = E_{osc}^{(d)}(n_\rho, |m|, \mu) + \langle i | \Delta V_1 | j \rangle + \langle i | \Delta V_2 | j \rangle + \langle i | V_g | j \rangle + \langle i | V_{\mathbf{\Omega s}} | j \rangle + \langle i | V_{\mathbf{\Omega}^2} | j \rangle \quad (81)$$

LEVEL SCHEMES AND SHELL EFFECTS

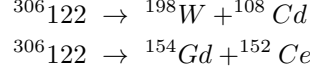
A ten shell scheme matrix elements have been calculated, which means a 440×440 matrix. After proper diagonalization, the levels are obtained.

First, DTCSM spectra are computed for the superheavy fission reaction channel $^{306}_{122} \rightarrow ^{198}W + ^{108}Cd$, with the nuclei deformations $\chi_{122} = 0.9$, $\chi_W = 1$. and $\chi_{Cd} = 0.83$. Semiaxes a_i and b_i are calculated from corresponding deformation parameter β_2 for every fragment, and using the volume conservation condition ($\beta_2^{198W} = 0.$, $\beta_2^{108Cd} = 0.135$ [10]). The reduced distance between centers is chosen to represent the elongation parameter of the shape : $(R - R_i)/(R_f - R_i)$, where R_i is the distance between centers when the light emerging fragment is completely embeded in the parent nucleus, and $R_f = a_1 + a_2 + 2R_3$ represents the final distance between centers, when the neck sphere is aligned with the fragments.

A direct consequence of the variation of the neck parameter R_3 on microscopic behaviour of a fission process is depicted in Fig. 6. Here the shell corections are drawn for the five R_3 - parameter values, as a function of the distance

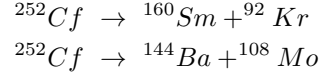
between centers. They are calculated with the Strutinsky method. A shallow minimum at $R \approx 2.5$ fm suggest a small deformation of the $^{306}_{122}$ ground state. First bump around $R \approx 5 - 6$ fm shows up in every case. Second bump is also there, but its position changes in R -value and in height (between $R=12$ fm and $R=20$ fm). The rather deep minimum (≈ -5 MeV) for large neck radii (apparent on the $R_3 = 10$ fm curve) is probably not manifested in $^{306}_{122}$ fission, since at this distance between centers, the system is out of the fission barrier due to strong Coulombian repulsion.

Second example takes into account the mass asymmetry parameter. Again is the fission of the superheavy $^{306}_{122}$ through two channels this time:



The two corresponding level schemes are on the upper side of Fig. 7 ($\chi_{Gd}=0.72$ for $\beta_2^{Gd}=0.243$ and $\chi_{Ce}=0.71$ for $\beta_2^{Ce}=0.261$). They have been chosen because of the mass symmetry of the second reaction against an asymmetric one. Calculations in this case preserved $R_3=4$ fm. Shells are more clearly visible at $(R - R_i)/(R_f - R_i)=1$ in the symmetric case, since asymptotically the levels are practically coincident for the two quasi-equal fragments. The lower part of the figure represents the shell corrections calculated with the above level schemes as an input. The first bump is shifted towards smaller R for symmetry. A second minimum as deep as almost the ground state along the symmetric channel is an indication of a possible shape isomer. Second maximum appears only for the asymmetric reaction. Asymptotically there is a $\Delta E \approx 4$ MeV difference in between the two channels, suggesting a possible fission path along the mass asymmetry degree of freedom.

The last studied case is the fission of ^{252}Cf ($\chi_{Cf}=0.73$ for $\beta_2^{Cf}=0.236$) through two favorized channels in Fig. 8:



These two reactions have been chosen because they lie within the maxima of the fission fragment mass distribution of ^{252}Cf [11]. The fragment deformation parameters considered in calculations are $\chi_{Sm}=0.68$ for $\beta_2^{Sm}=0.290$; $\chi_{Kr}=0.73$ for $\beta_2^{Kr}=0.228$; $\chi_{Ba}=0.8$ for $\beta_2^{Ba}=0.164$; $\chi_{Mo}=0.65$ for $\beta_2^{Mo}=0.333$. Level schemes are rather likely in the first part of the splitting, a fact that can be observed from the small differences in the shell corrections up to $R \approx 7$ fm. Beyond this distance between centers, the effect of the wells separation becomes more and more important, fragment individuality imposing the difference. If only for the shell corrections, $^{160}Sm + ^{92}Kr$ seem to be a more probable fission channel, but it beyond the purpose of this work to do a fission process analysis. Separation occurs around 18 fm, for approximately both of the reactions. As it is already known, lower energy shells of the fragments are the first to unveil asymptotically, whereas the higher states of the two systems still interact. This is an expected result since the potentials separate starting with the bottom of the wells, while the upper part of the potentials still overlap.

CONCLUSIONS

The deformed two-center shell model presented in this work describes the evolution of single particle levels from one parent potential well to the two fragments ones.

The introduction of fragment ellipsoidal deformation in the two-center oscillator wells and further on, in the spin-orbit and \mathbf{l}^2 operators enables a more realistic calculation of the two interacting quantum systems. This new form of spin-orbit $\mathbf{\Omega s}$ and $\mathbf{\Omega}^2$ allows for the angular momentum dependent operators to follow the exact sequence of shapes throughout the splitting process. In such a way ellipsoidal degrees of freedom are considered within spin-orbit interaction.

The new necking-in dependent microscopic potential results in considering the neck degree of freedom into the level scheme calculation. As has been shown, the last part of the fission process is influenced by the difference in neck radii. This fact has important consequences on the potential barriers and fission paths on a potential energy surface calculated within more deformation degrees of freedom, necking included.

A new way of treating two partially overlapping nuclei has been introduced by making use of matching potential surfaces. It is only in this way that *continuity* between different regions of potential influence is assured. The potential pass smoothly from V_1 to V_g , to V_2 and so on without any cusp in its value and without the introduction of arbitrary geometric transition functions. For zero neck radius one obtains the fusion-like type of shapes.

All these facts make the presented model suitable for the study of fission channels and cluster decay phenomena and calculation of potential energy surfaces in fission.

Also the model provides the analysis of possible deformed target-projectile doors toward fusion processes in heavy ion reactions. In nucleus-nucleus collisions, calculations of two fusing deformed partners yield the single particle spectra for the important (yet avoided up to now) region of overlapping shapes.

DTCSM OSCILLATOR MATRIX ELEMENTS

Formulas for the two deformed oscillators with necking-in are presented to enable $\langle'|\Delta V_1|\rangle$, $\langle'|\Delta V_2|\rangle$ and $\langle'|\Delta V_g|\rangle$ matrix elements to be calculated. The spin-dependent part is not included, since it introduce only a $\delta_{s's}$ factor.

We preserve the same notations as in section 6. $\langle i|j\rangle_\alpha^\beta$ stands for the integral calculated from α to β limits; $|n_z\rangle$ is the $Z_{\nu_{n_z}}(z)$ wave function; $|n_\rho m n_z\rangle$ is the total $\Phi_m R_{n_\rho}^{m|} Z_{\nu_{n_z}}$ wave function of the basis.

The following notations will be available from now on:

$$I(n'_\rho, n_\rho, m', m, m'_g, m_g, m_p, t) = \left[\frac{\Gamma(n'_\rho + 1)\Gamma(n_\rho + 1)}{\Gamma(n'_\rho + m'_g)\Gamma(n_\rho + m_g)} \right]^{\frac{1}{2}} \int_t^\infty e^{-x} x^{m_p} L_{n'_\rho}^{m'}(x) L_{n_\rho}^m(x) dx \quad (82)$$

which is computed by Gauss-Laguerre numerical integration procedure, and:

$$G(n'_\rho, n_\rho, m', m, t) = \left[\frac{\Gamma(n'_\rho + 1)\Gamma(n_\rho + 1)}{\Gamma(n'_\rho + |m'| + 1)\Gamma(n_\rho + |m| + 1)} \right]^{\frac{1}{2}} 2\alpha_1 t^{m+m'+\frac{1}{2}} e^{-t} L_{n'_\rho}^{m'}(t) L_{n_\rho}^m(t) \quad (83)$$

where:

$$\alpha_{\rho_i} = \left(\frac{m_0 \omega_{\rho_i}}{\hbar} \right)^{\frac{1}{2}} \quad \alpha_{z_i} = \left(\frac{m_0 \omega_{z_i}}{\hbar} \right)^{\frac{1}{2}} \quad \alpha_1 = \left(\frac{m_0 \omega_1}{\hbar} \right)^{\frac{1}{2}} \quad (84)$$

where ω_1 is the corresponding frequency for the sphere with the same volume. Relations between ellipsoids frequencies and the one for the sphere can easily be obtained from volume conservation $ab^2 = R_i^3$, when a, b are the semiaxes of the ellipse and R_i the radius of the sphere having the same volume. So the deformation shape dependence is contained in α_i factors. Also:

$$\langle i|f(\rho, z)|j\rangle_a^b \quad (85)$$

means that the integral is performed between the limits a and b .

$$\langle i|f(\rho, z)|j\rangle(z=c) \quad (86)$$

means the integrand is taken at the variable value $z = c$. This last kind of expressions intervene when the spin-orbit differentiation operators act on the Heavyside $\theta(z)$ function, resulting the $\delta(z)$ function.

We have for ΔV_1 :

$$\begin{aligned} \langle n'_\rho m' n'_z | \Delta V_1^{(p)} | n_\rho m n_z \rangle = & \\ & \frac{1}{2} (m_0 \omega_{\rho_1}^2 - m_0 \omega_1^2) (\langle n'_z | n_z \rangle_{-\infty}^{z_{im}} + \langle n'_z | n_z \rangle_{z_{0m}+a_m}^\infty \\ & \cdot \frac{1}{\alpha_1^2} [(2n_\rho + |m| + 1) \delta_{n'_\rho n_\rho} - \sqrt{n_\rho(n_\rho + |m|)} \delta_{n'_\rho n_\rho - 1} - \sqrt{(n_\rho + 1)(n_\rho + |m| + 1)} \delta_{n'_\rho n_\rho + 1}] \\ & + \frac{1}{2} [(m_0 \omega_{z_1}^2 - m_0 \omega_1^2) \langle n'_z | (z + z_1)^2 | n_z \rangle_{-\infty}^{z_{im}} + m_0 \omega_{z_1}^2 \langle n'_z | (z + z_1)^2 | n_z \rangle_{z_{0m}+a_m}^\infty \\ & - m_0 \omega_2^2 \langle n'_z | (z - z_2)^2 | n_z \rangle_{z_{0m}+a_m}^\infty] \delta_{n'_\rho n_\rho} \\ & + \frac{1}{2} (m_0 \omega_{\rho_1}^2 - m_0 \omega_1^2) (\langle n'_z | n_z \rangle_{z_{im}}^0 + \langle n'_z | n_z \rangle_0^{z_{0m}+a_m}) \end{aligned}$$

$$\begin{aligned}
& \cdot \frac{1}{\alpha_1^2} I(n'_\rho, n_\rho, |m|, |m|, |m|+1, |m|+1, |m|+1, \alpha_1^2 \rho_m^2(z)) \\
& + \frac{1}{2} [(m_0 \omega_{z_1}^2 - m_0 \omega_1^2) \langle n'_z | (z+z_1)^2 | n_z \rangle_{z_{im}}^0 + m_0 \omega_{z_1}^2 \langle n'_z | (z+z_1)^2 | n_z \rangle_0^{z_{0m}+a_m} \\
& - m_0 \omega_2^2 \langle n'_z | (z-z_2)^2 | n_z \rangle_0^{z_{0m}+a_m}] \cdot I(n'_\rho, n_\rho, |m|, |m|, |m|+1, |m|+1, |m|, \alpha_1^2 \rho_m^2(z))
\end{aligned} \tag{87}$$

For the *minus* terms in ΔV_1 :

$$\begin{aligned}
& \langle n'_\rho m' n'_z | \Delta V_1(z_i \div z_f; \rho_i \div \rho_f) | n_\rho m n_z \rangle = \\
& \frac{1}{2} m_0 \omega_{\rho_1}^2 \langle n'_z | n_z \rangle_{z_i}^{z_f} \frac{1}{\alpha_1^2} [I(n'_\rho, n_\rho, |m|, |m|, |m|+1, |m|+1, |m|+1, \alpha_1^2 \rho_i^2(z)) \\
& - I(n'_\rho, n_\rho, |m|, |m|, |m|+1, |m|+1, |m|+1, \alpha_1^2 \rho_f^2(z))] \\
& + \frac{1}{2} m_0 \omega_{z_1}^2 \langle n'_z | (z+z_1)^2 | n_z \rangle_{z_i}^{z_f} [I(n'_\rho, n_\rho, |m|, |m|, |m|+1, |m|+1, |m|, \alpha_1^2 \rho_i^2(z)) \\
& - I(n'_\rho, n_\rho, |m|, |m|, |m|+1, |m|+1, |m|, \alpha_1^2 \rho_f^2(z))]
\end{aligned} \tag{88}$$

Matrix elements for ΔV_2 reads:

$$\begin{aligned}
& \langle n'_\rho m' n'_z | \Delta V_2^{(p)} | n_\rho m n_z \rangle = \\
& \frac{1}{2} (m_0 \omega_{\rho_2}^2 - m_0 \omega_1^2) (\langle n'_z | n_z \rangle_{z_{im}}^0 + \langle n'_z | n_z \rangle_0^{z_{0m}+a_m}) \\
& \cdot \frac{1}{\alpha_1^2} [(2n_\rho + |m| + 1) \delta_{n'_\rho, n_\rho} - \sqrt{n_\rho(n_\rho + |m|)} \delta_{n'_\rho, n_\rho-1} - \sqrt{(n_\rho+1)(n_\rho + |m| + 1)} \delta_{n'_\rho, n_\rho+1} \\
& - I(n'_\rho, n_\rho, |m|, |m|, |m|+1, |m|+1, |m|+1, \alpha_1^2 \rho_m^2(z))] \\
& + \frac{1}{2} [m_0 \omega_{z_2}^2 \langle n'_z | (z-z_2)^2 | n_z \rangle_{z_{im}}^0 - m_0 \omega_1^2 \langle n'_z | (z+z_1)^2 | n_z \rangle_{z_{im}}^0 \\
& - (m_0 \omega_{z_2}^2 - m_0 \omega_2^2) \langle n'_z | (z-z_2)^2 | n_z \rangle_0^{z_{0m}+a_m}] \\
& \cdot [\delta_{n'_\rho, n_\rho} - I(n'_\rho, n_\rho, |m|, |m|, |m|+1, |m|+1, |m|, \alpha_1^2 \rho_m^2(z))]
\end{aligned} \tag{89}$$

and again for the *minus* terms in ΔV_2 :

$$\begin{aligned}
& \langle n'_\rho m' n'_z | \Delta V_2(z_i \div z_f; \rho_i \div \rho_f) | n_\rho m n_z \rangle = \\
& \frac{1}{2} m_0 \omega_{\rho_2}^2 \langle n'_z | n_z \rangle_{z_i}^{z_f} \frac{1}{\alpha_1^2} [I(n'_\rho, n_\rho, |m|, |m|, |m|+1, |m|+1, |m|+1, \alpha_1^2 \rho_i^2(z)) \\
& - I(n'_\rho, n_\rho, |m|, |m|, |m|+1, |m|+1, |m|+1, \alpha_1^2 \rho_f^2(z))] \\
& + \frac{1}{2} m_0 \omega_{z_2}^2 \langle n'_z | (z-z_2)^2 | n_z \rangle_{z_i}^{z_f} [I(n'_\rho, n_\rho, |m|, |m|, |m|+1, |m|+1, |m|, \alpha_1^2 \rho_i^2(z)) \\
& - I(n'_\rho, n_\rho, |m|, |m|, |m|+1, |m|+1, |m|, \alpha_1^2 \rho_f^2(z))]
\end{aligned} \tag{90}$$

And finally for the neck potential operators, the expressions for the matrix elements are:

$$\begin{aligned}
& \langle n'_\rho m' n'_z | V_{g1}(z_i \div z_f; \rho_i \div \rho_f) | n_\rho m n_z \rangle = \\
& \left[\left(2V_0 - \frac{m_0 \omega_g^2}{2} \rho_3^2 \right) \langle n'_z | n_z \rangle_{z_i}^{z_f} - \frac{1}{2} m_0 \omega_g^2 \langle n'_z | (z-z_3)^2 | n_z \rangle_{z_i}^{z_f} \right] \\
& \cdot [I(n'_\rho, n_\rho, |m|, |m|, |m|+1, |m|+1, |m|, \alpha_1^2 \rho_i^2(z)) \\
& - \frac{1}{2} m_0 \omega_g^2 \langle n'_z | n_z \rangle_{z_i}^{z_f} \left\{ \frac{1}{\alpha_1^2} [I(n'_\rho, n_\rho, |m|, |m|, |m|+1, |m|+1, |m|+1, \alpha_1^2 \rho_i^2(z)) \right. \\
& \left. - I(n'_\rho, n_\rho, |m|, |m|, |m|+1, |m|+1, |m|+1, \alpha_1^2 \rho_f^2(z))] \right\}
\end{aligned}$$

$$\begin{aligned}
& -\frac{2\rho_3}{\alpha_1}[I(n'_\rho, n_\rho, |m|, |m|, |m|+1, |m|+1, |m|+\frac{1}{2}, \alpha_1^2\rho_i^2(z)) \\
& -I(n'_\rho, n_\rho, |m|, |m|, |m|+1, |m|+1, |m|+\frac{1}{2}, \alpha_1^2\rho_f^2(z))]\}
\end{aligned} \tag{91}$$

and:

$$\begin{aligned}
& \langle n'_\rho m' n'_z | V_{g2} | n_\rho m n_z \rangle = \\
& V_0 \{ \langle n'_z | n_z \rangle_{z_{c1}}^{z_s} [I(n'_\rho, n_\rho, |m|, |m|, |m|+1, |m|+1, |m|, \alpha_1^2\rho_1^2(z)) \\
& -I(n'_\rho, n_\rho, |m|, |m|, |m|+1, |m|+1, |m|, \alpha_1^2\rho_g^2(z))] \\
& + \langle n'_z | n_z \rangle_{z_s}^{z_{c2}} [I(n'_\rho, n_\rho, |m|, |m|, |m|+1, |m|+1, |m|, \alpha_1^2\rho_2^2(z)) \\
& -I(n'_\rho, n_\rho, |m|, |m|, |m|+1, |m|+1, |m|, \alpha_1^2\rho_g^2(z))] \}
\end{aligned} \tag{92}$$

For the z -dependent terms of the matrix elements, the following abbreviations are available [9] :

$$\begin{aligned}
j_{\nu_1, \nu_2, \zeta_i} &= \int_0^\infty d\zeta e^{-(\zeta-\zeta_i)^2} \mathcal{H}_{\nu_1}(\zeta-\zeta_i) \mathcal{H}_{\nu_2}(\zeta-\zeta_i) \\
& \int_{-\infty}^0 e^{-(\zeta+\zeta_i)^2} \mathcal{H}_{\nu_1}[-(\zeta+\zeta_i)] \mathcal{H}_{\nu_2}[-(\zeta+\zeta_i)] d\zeta
\end{aligned} \tag{93}$$

$$j_{\nu_1, \nu_2, \zeta_i - \zeta_0} = \int_{\zeta_0}^\infty e^{-(\zeta-\zeta_i)^2} \mathcal{H}_{\nu_1}(\zeta-\zeta_i) \mathcal{H}_{\nu_2}(\zeta-\zeta_i) d\zeta \tag{94}$$

where the general formula for computing these kind of intergals is:

$$j_{\nu_1, \nu_2, \zeta_0} = \frac{e^{-\zeta_0^2}}{\nu_1 - \nu_2} [\nu_1 \mathcal{H}_{\nu_1-1}(-\zeta_0) \mathcal{H}_{\nu_2}(-\zeta_0) - \nu_2 \mathcal{H}_{\nu_1}(-\zeta_0) \mathcal{H}_{\nu_2-1}(-\zeta_0)] \tag{95}$$

and $\mathcal{H}_\nu(\zeta)$ is the Hermite function.

$$\begin{aligned}
\langle n'_z | n_z \rangle_{z_i}^{z_f} &= C_{\nu'_1} C_{\nu_1} \frac{1}{\alpha_1} [j_{\nu'_1, \nu_1, \alpha_1(z_1+z_f)} - j_{\nu'_1, \nu_1, \alpha_1(z_1+z_i)}] \quad , z_i, z_f < 0 \\
&= C_{\nu'_2} C_{\nu_2} \frac{1}{\alpha_2} [j_{\nu'_2, \nu_2, \alpha_2(z_2-z_i)} - j_{\nu'_2, \nu_2, \alpha_2(z_2-z_f)}] \quad , z_i, z_f \geq 0
\end{aligned} \tag{96}$$

$$\begin{aligned}
\langle n'_z | (z+z_1)^2 | n_z \rangle_{z_i}^{z_f} &= C_{\nu'_1} C_{\nu_1} \frac{1}{\alpha_1^3} \left\{ \frac{1}{4} [j_{\nu'_1+1, \nu_1+1, \alpha_1(z_1+z_f)} - j_{\nu'_1+1, \nu_1+1, \alpha_1(z_1+z_i)}] \right. \\
& + \frac{\nu'_1}{2} [j_{\nu'_1+1, \nu_1-1, \alpha_1(z_1+z_f)} - j_{\nu'_1+1, \nu_1-1, \alpha_1(z_1+z_i)}] \\
& + \frac{\nu_1}{2} [j_{\nu'_1-1, \nu_1+1, \alpha_1(z_1+z_f)} - j_{\nu'_1-1, \nu_1+1, \alpha_1(z_1+z_i)}] \\
& \left. + \nu'_1 \nu_1 [j_{\nu'_1-1, \nu_1-1, \alpha_1(z_1+z_f)} - j_{\nu'_1-1, \nu_1-1, \alpha_1(z_1+z_i)}] \right\}
\end{aligned} \tag{97}$$

$$\begin{aligned}
\langle n'_z | (z-z_2)^2 | n_z \rangle_{z_i}^{z_f} &= C_{\nu'_2} C_{\nu_2} \frac{1}{\alpha_2^3} \left\{ \frac{1}{4} [j_{\nu'_2+1, \nu_2+1, \alpha_2(z_2-z_i)} - j_{\nu'_2+1, \nu_2+1, \alpha_2(z_2-z_f)}] \right. \\
& + \frac{\nu'_2}{2} [j_{\nu'_2+1, \nu_2-1, \alpha_2(z_2-z_i)} - j_{\nu'_2+1, \nu_2-1, \alpha_2(z_2-z_f)}] \\
& + \frac{\nu_2}{2} [j_{\nu'_2-1, \nu_2+1, \alpha_2(z_2-z_i)} - j_{\nu'_2-1, \nu_2+1, \alpha_2(z_2-z_f)}] \\
& \left. + \nu'_2 \nu_2 [j_{\nu'_2-1, \nu_2-1, \alpha_2(z_2-z_i)} - j_{\nu'_2-1, \nu_2-1, \alpha_2(z_2-z_f)}] \right\}
\end{aligned} \tag{98}$$

$$\begin{aligned} \langle n'_z | z + z_1 | n_z \rangle_{z_i}^{z_f} &= C_{\nu'_1} C_{\nu_1} \frac{1}{\alpha_1^2} \left\{ \frac{1}{2} [j_{\nu'_1, \nu_1+1, \alpha_1}(z_1+z_i) - j_{\nu'_1, \nu_1+1, \alpha_1}(z_1+z_f)] \right. \\ &\quad \left. + \nu_1 [j_{\nu'_1, \nu_1-1, \alpha_1}(z_1+z_i) - j_{\nu'_1, \nu_1-1, \alpha_1}(z_1+z_f)] \right\} \end{aligned} \quad (99)$$

$$\begin{aligned} \langle n'_z | z - z_2 | n_z \rangle_{z_i}^{z_f} &= C_{\nu'_2} C_{\nu_2} \frac{1}{\alpha_2^2} \left\{ \frac{1}{2} [j_{\nu'_2, \nu_2+1, \alpha_2}(z_2-z_i) - j_{\nu'_2, \nu_2+1, \alpha_2}(z_2-z_f)] \right. \\ &\quad \left. + \nu_2 [j_{\nu'_2, \nu_2-1, \alpha_2}(z_2-z_i) - j_{\nu'_2, \nu_2-1, \alpha_2}(z_2-z_f)] \right\} \end{aligned} \quad (100)$$

For $(z - z_3)$ dependent terms, one can use:

$$\langle n'_z | (z - z_3)^2 | n_z \rangle_{z_i}^{z_f} = \langle n'_z | (z - z_2)^2 | n_z \rangle_{z_i}^{z_f} + 2(z_2 - z_3) \langle n'_z | z - z_2 | n_z \rangle_{z_i}^{z_f} + (z_2 - z_3)^2 \langle n'_z | n_z \rangle_{z_i}^{z_f} \quad (101)$$

$$\begin{aligned} &\left\langle n'_z \left| \frac{\partial}{\partial z} \right| n_z \right\rangle_{z_i}^{z_f} = \\ &= C_{\nu'_1} C_{\nu_1} \left[\frac{1}{2} (j_{\nu'_1, \nu_1+1, \alpha_1}(z_1+z_f) - j_{\nu'_1, \nu_1+1, \alpha_1}(z_1+z_i)) \right. \\ &\quad \left. + \nu_1 (j_{\nu'_1, \nu_1-1, \alpha_1}(z_1+z_f) - j_{\nu'_1, \nu_1-1, \alpha_1}(z_1+z_i)) \right] \quad z_i, z_f < 0 \\ &= C_{\nu'_2} C_{\nu_2} \left[-\frac{1}{2} (j_{\nu'_2, \nu_2+1, \alpha_2}(z_2-z_i) - j_{\nu'_2, \nu_2+1, \alpha_2}(z_2-z_f)) \right. \\ &\quad \left. + \nu_2 (j_{\nu'_2, \nu_2-1, \alpha_2}(z_2-z_i) - j_{\nu'_2, \nu_2-1, \alpha_2}(z_2-z_f)) \right] \quad z_i, z_f \geq 0 \end{aligned} \quad (102)$$

SPIN-ORBIT AND Ω^2 MATRIX ELEMENTS

The necessary expressions to calculate the matrix elements for spin-orbit and Ω^2 terms are given in this appendix. For the (v_1) volume, we use the abbreviation:

$$\begin{aligned} w_1(v_1) &= (\sqrt{n_\rho + 1} \delta_{n_\rho, n_\rho+1} + \sqrt{n_\rho + |m|} \delta_{n_\rho, n_\rho}) 2m_0 \omega_{z_1}^2 \alpha_1 \\ &\quad \cdot (\langle n'_z | z + z_1 | n_z \rangle_{-\infty}^{z_{im}} + \langle n'_z | z + z_1 | n_z \rangle_{z_{0m}+a_m}^\infty \\ &\quad + (\sqrt{n_\rho + 1} \delta_{n_\rho, n_\rho+1} - \sqrt{n_\rho + |m|} \delta_{n_\rho, n_\rho}) \cdot \frac{m_0 \omega_{\rho_1}^2}{\alpha_1} \\ &\quad \cdot \left[2 \left(\left\langle n'_z \left| \frac{\partial}{\partial z} \right| n_z \right\rangle_{-\infty}^{z_{im}} + \left\langle n'_z \left| \frac{\partial}{\partial z} \right| n_z \right\rangle_{z_{0m}+a_m}^\infty \right) \right. \\ &\quad \left. + \langle n'_z | n_z \rangle(z = z_{0m} + a_m) - \langle n'_z | n_z \rangle(z = z_{im}) \right] \end{aligned} \quad (103)$$

$$\begin{aligned} w_2(v_1) &= (\sqrt{n_\rho + |m|} + 1 \delta_{n'_\rho, n_\rho} + \sqrt{n_\rho} \delta_{n'_\rho, n_\rho-1}) \cdot 2m_0 \omega_{z_1}^2 \alpha_1 \\ &\quad \cdot (\langle n'_z | z + z_1 | n_z \rangle_{-\infty}^{z_{im}} + \langle n'_z | z + z_1 | n_z \rangle_{z_{0m}+a_m}^\infty) \\ &\quad + (\sqrt{n_\rho + |m|} + 1 \delta_{n'_\rho, n_\rho} - \sqrt{n_\rho} \delta_{n'_\rho, n_\rho-1}) \cdot \frac{m_0 \omega_{\rho_1}^2}{\alpha_1} \\ &\quad \cdot \left[2 \left(\left\langle n'_z \left| \frac{\partial}{\partial z} \right| n_z \right\rangle_{-\infty}^{z_{im}} + \left\langle n'_z \left| \frac{\partial}{\partial z} \right| n_z \right\rangle_{z_{0m}+a_m}^\infty \right) \right. \\ &\quad \left. + \langle n'_z | n_z \rangle(z = z_{0m} + a_m) - \langle n'_z | n_z \rangle(z = z_{im}) \right] \end{aligned} \quad (104)$$

Then we have:

$$\begin{aligned}
\langle n'_\rho m' n'_z | \{ \mathbf{\Omega}^+(v_1), [1 - \theta(z - z_{im})] + \{ \mathbf{\Omega}^+(v_1), [z - (z_{0m} + a_m)] \} \} | n_\rho m n_z \rangle \\
= \delta_{m'm+1} \cdot w_1(v_1) \quad , m < 0 \\
= \delta_{m'm+1} \cdot (-w_2(v_1)) \quad , m \geq 0
\end{aligned} \tag{105}$$

$$\begin{aligned}
\langle n'_\rho m' n'_z | \{ \mathbf{\Omega}^-(v_1), [1 - \theta(z - z_{im})] + \{ \mathbf{\Omega}^+(v_1), [z - (z_{0m} + a_m)] \} \} | n_\rho m n_z \rangle \\
= \delta_{m'm-1} \cdot w_2(v_1) \quad , m \leq 0 \\
= \delta_{m'm-1} \cdot (-w_1(v_1)) \quad , m > 0
\end{aligned} \tag{106}$$

Because of the symmetry we have:

$$\langle ' | \{ \mathbf{\Omega}^+, f(\rho, z) \} | \rangle (m', m) = \langle | \{ \mathbf{\Omega}^-, f(\rho, z) \} | ' \rangle (m, m') \tag{107}$$

So, only one half of the $\mathbf{\Omega}$ s and $\mathbf{\Omega}^2$ matrix elements must be calculated. Further on, only the $\mathbf{\Omega}^+$ matrix elements are given, the $\mathbf{\Omega}^-$ part resulting from symmetry.

$$\begin{aligned}
\langle n'_\rho m' n'_z | \{ \mathbf{\Omega}^+(v_1), [\theta(z - z_{im}) - \theta[z - (z_{0m} + a_m)]] \theta(\rho - \rho_m(z)) \} | n_\rho m n_z \rangle = \\
\delta_{m'm+1} \{ -I(n'_\rho, n_\rho, |m| - 1, |m|, |m|, |m| + 1, |m|, \alpha_1^2 \rho_m^2(z)) \\
\cdot \left[2m_0 \omega_{z_1}^2 \alpha_1 \langle n'_z | z + z_1 | n_z \rangle_{z_{im}}^{z_{0m} + a_m} \right. \\
+ \frac{m_0 \omega_{\rho_1}^2}{\alpha_1} \left(2 \left\langle n'_z \left| \frac{\partial}{\partial z} \right| n_z \right\rangle_{z_{im}}^{z_{0m} + a_m} + \langle n'_z | n_z \rangle (z = z_{im}) - \langle n'_z | n_z \rangle (z = z_{0m} + a_m) \right) \Big] \\
+ 2m_0 \omega_{z_1}^2 \alpha_1 \langle n'_z | z + z_1 | n_z \rangle_{z_{im}}^{z_{0m} + a_m} \\
\cdot [2(n_\rho + |m|)I(n'_\rho, n_\rho, |m| - 1, |m| - 1, |m|, |m| + 1, |m| - 1, \alpha_1^2 \rho_m^2(z)) \\
+ \frac{1}{2\alpha_1} G(n'_\rho, n_\rho, |m| - 1, |m|, \alpha_1^2 \rho_m^2(z))] \} \quad , m < 0
\end{aligned} \tag{108}$$

$$\tag{109}$$

and:

$$\begin{aligned}
\langle n'_\rho m' n'_z | \{ \mathbf{\Omega}^+(v_1), [\theta(z - z_{im}) - \theta[z - (z_{0m} + a_m)]] \theta(\rho - \rho_m(z)) \} | n_\rho m n_z \rangle = \\
\delta_{m'm+1} \{ I(n'_\rho, n_\rho, |m| + 1, |m|, |m| + 2, |m| + 1, |m| + 1, \alpha_1^2 \rho_m^2(z)) \\
\cdot \left[2m_0 \omega_{z_1}^2 \alpha_1 \langle n'_z | z + z_1 | n_z \rangle_{z_{im}}^{z_{0m} + a_m} \right. \\
- \frac{m_0 \omega_{\rho_1}^2}{\alpha_1} \left(2 \left\langle n'_z \left| \frac{\partial}{\partial z} \right| n_z \right\rangle_{z_{im}}^{z_{0m} + a_m} + \langle n'_z | n_z \rangle (z = z_{im}) - \langle n'_z | n_z \rangle (z = z_{0m} + a_m) \right) \Big] \\
- 2m_0 \omega_{z_1}^2 \alpha_1 \langle n'_z | z + z_1 | n_z \rangle_{z_{im}}^{z_{0m} + a_m} \\
\cdot [2I(n'_\rho, n_\rho, |m| + 1, |m| + 1, |m| + 2, |m| + 1, |m| + 1, \alpha_1^2 \rho_m^2(z)) \\
+ \frac{1}{2\alpha_1} G(n'_\rho, n_\rho, |m| + 1, |m|, \alpha_1^2 \rho_m^2(z))] \} \quad , m \geq 0
\end{aligned} \tag{110}$$

$$\begin{aligned}
\langle n'_\rho m' n'_z | \{ \mathbf{\Omega}^+(v_1), [\theta(z - z_i) - \theta(z - z_f)] [\theta(\rho - \rho_i(z)) - \theta(\rho - \rho_f(z))] \} | n_\rho m n_z \rangle = \\
\delta_{m'm+1} \{ [-I(n'_\rho, n_\rho, |m| - 1, |m|, |m|, |m| + 1, |m|, \alpha_1^2 \rho_i^2(z)) \\
+ I(n'_\rho, n_\rho, |m| - 1, |m|, |m|, |m| + 1, |m|, \alpha_1^2 \rho_f^2(z))] \\
\cdot \left[2m_0 \omega_{z_1}^2 \alpha_1 \langle n'_z | z + z_1 | n_z \rangle_{z_i}^{z_f} \right. \\
+ \frac{m_0 \omega_{\rho_1}^2}{\alpha_1} \left(2 \left\langle n'_z \left| \frac{\partial}{\partial z} \right| n_z \right\rangle_{z_i}^{z_f} + \langle n'_z | n_z \rangle (z = z_i) - \langle n'_z | n_z \rangle (z = z_f) \right) \Big]
\end{aligned}$$

$$\begin{aligned}
& +2m_0\omega_{z_1}^2\alpha_1\langle n'_z|z+z_1|n_z\rangle_{z_i}^{z_f} \\
& \cdot[2(n_\rho+|m|)I(n'_\rho,n_\rho,|m|-1,|m|-1,|m|,|m|+1,|m|-1,\alpha_1^2\rho_i^2(z)) \\
& -I(n'_\rho,n_\rho,|m|-1,|m|-1,|m|,|m|+1,|m|-1,\alpha_1^2\rho_f^2(z))] \\
& +\frac{1}{2\alpha_1}[G(n'_\rho,n_\rho,|m|-1,|m|,\alpha_1^2\rho_1^2(z))-G(n'_\rho,n_\rho,|m|-1,|m|,\alpha_1^2\rho_f^2(z))]\} \\
& , m < 0
\end{aligned} \tag{111}$$

and the same term for $m \geq 0$:

$$\begin{aligned}
& \langle n'_\rho m' n'_z | \{ \mathbf{\Omega}^+(v_1), [\theta(z-z_i) - \theta(z-z_f)][\theta(\rho-\rho_i(z)) - \theta(\rho-\rho_f(z))]\} | n_\rho m n_z \rangle = \\
& \delta_{m'+m+1} \{ [I(n'_\rho, n_\rho, |m|+1, |m|, |m|+2, |m|+1, |m|+1, \alpha_1^2\rho_i^2(z)) \\
& - I(n'_\rho, n_\rho, |m|+1, |m|, |m|+2, |m|+1, |m|+1, \alpha_1^2\rho_f^2(z))] \\
& \cdot \left[2m_0\omega_{z_1}^2\alpha_1\langle n'_z|z+z_1|n_z\rangle_{z_i}^{z_f} \right. \\
& \left. - \frac{m_0\omega_{\rho_1}^2}{\alpha_1} \left(2\langle n'_z | \frac{\partial}{\partial z} | n_z \rangle_{z_i}^{z_f} + \langle n'_z | n_z \rangle(z=z_i) - \langle n'_z | n_z \rangle(z=z_f) \right) \right] \\
& - 2m_0\omega_{z_1}^2\alpha_1\langle n'_z|z+z_1|n_z\rangle_{z_i}^{z_f} \\
& \cdot [2(I(n'_\rho, n_\rho, |m|+1, |m|+1, |m|+2, |m|+1, |m|+1, \alpha_1^2\rho_i^2(z)) \\
& - I(n'_\rho, n_\rho, |m|+1, |m|+1, |m|+2, |m|+1, |m|+1, \alpha_1^2\rho_f^2(z)) \\
& - \frac{1}{2\alpha_1}(G(n'_\rho, n_\rho, |m|+1, |m|, \alpha_1^2\rho_i^2(z)) - G(n'_\rho, n_\rho, |m|+1, |m|, \alpha_1^2\rho_f^2(z)))] \} \\
& , m \geq 0
\end{aligned} \tag{112}$$

$$\langle n'_\rho m' n'_z | \mathbf{\Omega}_z(v_1) | n_\rho m n_z \rangle = m_0\omega_{\rho_1}^2 m \delta_{m'm} \tag{113}$$

We now present the (v_2) -dependent necessary terms for $\mathbf{\Omega s}(v_2)$ matrix elements construction:

$$\begin{aligned}
& \langle n'_\rho m' n'_z | \{ \mathbf{\Omega}^+(v_2), [\theta(z-z_{im}) - \theta(z-(z_{0m}+a_m))][1 - \theta(\rho-\rho_m(z))]\} | n_\rho m n_z \rangle = \\
& \delta_{m'+m+1} \left\{ 2m_0\omega_{z_2}^2\alpha_1\langle n'_z|z-z_2|n_z\rangle_{z_{im}}^{z_{0m}+a_m} (\sqrt{n_\rho+|m|}\delta_{n'_\rho n_\rho} + \sqrt{n_\rho+1}\delta_{n'_\rho n_\rho+1}) \right. \\
& - \frac{m_0\omega_{\rho_2}^2}{2} \left(2\langle n'_z | \frac{\partial}{\partial z} | n_z \rangle_{z_{im}}^{z_{0m}+a_m} + \langle n'_z | n_z \rangle(z=z_{im}) - \langle n'_z | n_z \rangle(z=z_{0m}+a_m) \right) \\
& \cdot (\sqrt{n_\rho+|m|}\delta_{n'_\rho n_\rho} - \sqrt{n_\rho+1}\delta_{n'_\rho n_\rho+1}) \\
& + I(n'_\rho, n_\rho, |m|-1, |m|, |m|, |m|+1, |m|, \alpha_1^2\rho_m^2(z)) \\
& \cdot \left[2m_0\omega_{z_2}^2\alpha_1\langle n'_z|z-z_2|n_z\rangle_{z_{im}}^{z_{0m}+a_m} \right. \\
& + \frac{m_0\omega_{\rho_2}^2}{\alpha_1} \left(2\langle n'_z | \frac{\partial}{\partial z} | n_z \rangle_{z_{im}}^{z_{0m}+a_m} + \langle n'_z | n_z \rangle(z=z_{im}) - \langle n'_z | n_z \rangle(z=z_{0m}+a_m) \right) \\
& - 2m_0\omega_{z_2}^2\alpha_1\langle n'_z|z-z_2|n_z\rangle_{z_{im}}^{z_{0m}+a_m} \\
& \cdot [2(n_\rho+|m|)I(n'_\rho, n_\rho, |m|-1, |m|-1, |m|, |m|+1, |m|-1, \alpha_1^2\rho_m^2(z)) \\
& + \frac{1}{2\alpha_1}G(n'_\rho, n_\rho, |m|-1, |m|, \alpha_1^2\rho_m^2(z))] \} , m < 0
\end{aligned} \tag{114}$$

$$\begin{aligned}
& \langle n'_\rho m' n'_z | \{ \mathbf{\Omega}^+(v_2), [\theta(z-z_{im}) - \theta(z-(z_{0m}+a_m))][1 - \theta(\rho-\rho_m(z))]\} | n_\rho m n_z \rangle = \\
& \delta_{m'+m+1} \left\{ -2m_0\omega_{z_2}^2\alpha_1\langle n'_z|z-z_2|n_z\rangle_{z_{im}}^{z_{0m}+a_m} (\sqrt{n_\rho+|m|+1}\delta_{n'_\rho n_\rho} + \sqrt{n_\rho}\delta_{n'_\rho n_\rho-1}) \right.
\end{aligned}$$

$$\begin{aligned}
& -\frac{m_0\omega_{\rho_2}^2}{\alpha_1} \left(2 \left\langle n'_z \left| \frac{\partial}{\partial z} \right| n_z \right\rangle_{z_{im}}^{z_{0m}+a_m} + \langle n'_z | n_z \rangle (z = z_{im}) - \langle n'_z | n_z \rangle (z = z_{0m} + a_m) \right) \\
& \cdot (\sqrt{n_\rho + |m| + 1} \delta_{n'_\rho, n_\rho} - \sqrt{n_\rho} \delta_{n'_\rho, n_\rho - 1}) \\
& - I(n'_\rho, n_\rho, |m| + 1, |m|, |m| + 2, |m| + 1, |m| + 1, \alpha_1^2 \rho_m^2(z)) \\
& \cdot \left[2m_0\omega_{z_2}^2 \alpha_1 \langle n'_z | z - z_2 | n_z \rangle_{z_{im}}^{z_{0m}+a_m} \right. \\
& \left. - \frac{m_0\omega_{\rho_2}^2}{\alpha_1} \left(2 \left\langle n'_z \left| \frac{\partial}{\partial z} \right| n_z \right\rangle_{z_{im}}^{z_{0m}+a_m} + \langle n'_z | n_z \rangle (z = z_{im}) - \langle n'_z | n_z \rangle (z = z_{0m} + a_m) \right) \right] \\
& + 2m_0\omega_{z_2}^2 \alpha_1 \langle n'_z | z - z_2 | n_z \rangle_{z_{im}}^{z_{0m}+a_m} \\
& \cdot [2I(n'_\rho, n_\rho, |m| + 1, |m| + 1, |m| + 2, |m| + 1, |m| + 1, \alpha_1^2 \rho_m^2(z)) \\
& - \frac{1}{2\alpha_1} G(n'_\rho, n_\rho, |m| + 1, |m|, \alpha_1 \rho_m^2(z))] \Big\} , m \geq 0
\end{aligned} \tag{115}$$

$$\begin{aligned}
& \langle n'_\rho m' n'_z | \{ \Omega^+(v_2), [\theta(z - z_i) - \theta(z - z_f)] [\theta(\rho - \rho_i(z)) \theta(\rho - \rho_f(z))] \} | n_\rho m n_z \rangle = \\
& \delta_{m'm+1} \Big\{ [-I(n'_\rho, n_\rho, |m| - 1, |m|, |m|, |m| + 1, |m|, \alpha_1^2 \rho_i^2(z)) \\
& + I(n'_\rho, n_\rho, |m| - 1, |m|, |m|, |m| + 1, |m|, \alpha_1^2 \rho_f^2(z))] \\
& \cdot \left[2m_0\omega_{z_2}^2 \alpha_1 \langle n'_z | z - z_2 | n_z \rangle_{z_i}^{z_f} \right. \\
& + \frac{m_0\omega_{\rho_2}^2}{\alpha_1} \left(2 \left\langle n'_z \left| \frac{\partial}{\partial z} \right| n_z \right\rangle_{z_i}^{z_f} + \langle n'_z | n_z \rangle (z = z_i) - \langle n'_z | n_z \rangle (z = z_f) \right) \Big] \\
& + 2m_0\omega_{z_2}^2 \alpha_1 \langle n'_z | z - z_2 | n_z \rangle_{z_i}^{z_f} \\
& \cdot [2(n_\rho + |m|)(I(n'_\rho, n_\rho, |m| - 1, |m| - 1, |m|, |m| + 1, |m| - 1, \alpha_1^2 \rho_i^2(z)) \\
& - I(n'_\rho, n_\rho, |m| - 1, |m| - 1, |m|, |m| + 1, |m| - 1, \alpha_1^2 \rho_f^2(z))) \\
& + \frac{1}{2\alpha_1} (G(n'_\rho, n_\rho, |m| - 1, |m|, \alpha_1^2 \rho_i^2(z)) - G(n'_\rho, n_\rho, |m| - 1, |m|, \alpha_1^2 \rho_f^2(z)))] \Big\} \\
& , m < 0
\end{aligned} \tag{116}$$

$$\begin{aligned}
& \langle n'_\rho m' n'_z | \{ \Omega^+(v_2), [\theta(z - z_i) - \theta(z - z_f)] [\theta(\rho - \rho_i(z)) \theta(\rho - \rho_f(z))] \} | n_\rho m n_z \rangle = \\
& \delta_{m'm+1} \Big\{ [I(n'_\rho, n_\rho, |m| + 1, |m|, |m| + 2, |m| + 1, |m| + 1, \alpha_1^2 \rho_i^2(z)) \\
& - I(n'_\rho, n_\rho, |m| + 1, |m|, |m| + 2, |m| + 2, |m| + 1, |m| + 1, \alpha_1^2 \rho_f^2(z))] \\
& \cdot \left[2m_0\omega_{z_2}^2 \alpha_1 \langle n'_z | z - z_2 | n_z \rangle_{z_i}^{z_f} \right. \\
& - \frac{m_0\omega_{\rho_2}^2}{\alpha_1} \left(2 \left\langle n'_z \left| \frac{\partial}{\partial z} \right| n_z \right\rangle_{z_i}^{z_f} + \langle n'_z | n_z \rangle (z = z_i) - \langle n'_z | n_z \rangle (z = z_f) \right) \Big] \\
& - 2m_0\omega_{z_2}^2 \alpha_1 \langle n'_z | z - z_2 | n_z \rangle_{z_i}^{z_f} \\
& \cdot [2(I(n'_\rho, n_\rho, |m| + 1, |m| + 1, |m| + 2, |m| + 1, |m| + 1, \alpha_1^2 \rho_i^2(z)) \\
& - I(n'_\rho, n_\rho, |m| + 1, |m| + 1, |m| + 2, |m| + 1, |m| + 1, \alpha_1^2 \rho_f^2(z))) \\
& - \frac{1}{2\alpha_1} (G(n'_\rho, n_\rho, |m| + 1, |m|, \alpha_1^2 \rho_i^2(z)) - G(n'_\rho, n_\rho, |m| + 1, |m|, \alpha_1^2 \rho_f^2(z)))] \Big\} \\
& , m \geq 0
\end{aligned} \tag{117}$$

The diagonal term generated by Ω_z is:

$$\langle n'_\rho m' n'_z | \Omega_z(v_2) | n_\rho m n_z \rangle = m_0\omega_{\rho_2}^2 m \delta_{m'm} \tag{118}$$

For the neck region elements we have:

$$\begin{aligned}
& \langle n'_\rho m' n'_z | \{ \mathbf{\Omega}^+(v_{g1}), [\theta(z - z_i) - \theta(z - z_f)] [\theta(\rho - \rho_i(z)) - \theta(\rho - \rho_f(z))] \} | n_\rho m n_z \rangle = \\
& \delta_{m'm+1} m_0 \omega_g^2 \left\{ \frac{1}{\alpha_1} [I(n'_\rho, n_\rho, |m| - 1, |m|, |m|, |m| + 1, |m|, \alpha_1^2 \rho_i^2(z)) \right. \\
& - I(n'_\rho, n_\rho, |m| - 1, |m|, |m|, |m| + 1, |m|, \alpha_1^2 \rho_f^2(z))] \\
& - \rho_3 [I(n'_\rho, n_\rho, |m| - 1, |m|, |m|, |m| + 1, |m| - \frac{1}{2}, \alpha_1^2 \rho_i^2(z)) \\
& - I(n'_\rho, n_\rho, |m| - 1, |m|, |m|, |m| + 1, |m| - \frac{1}{2}, \alpha_1^2 \rho_f^2(z))] \} \\
& \cdot \left[2 \left\langle n'_z \left| \frac{\partial}{\partial z} \right| n_z \right\rangle_{z_i}^{z_f} + \langle n'_z | n_z \rangle (z = z_i) - \langle n'_z | n_z \rangle (z = z_f) \right] \\
& - 2 \{ \alpha_1 \{ 2(n_\rho + |m|) [I(n'_\rho, n_\rho, |m| - 1, |m| - 1, |m|, |m| + 1, |m| - 1, \alpha_1^2 \rho_i^2(z)) \\
& - I(n'_\rho, n_\rho, |m| - 1, |m| - 1, |m|, |m| + 1, |m| - 1, \alpha_1^2 \rho_f^2(z))] \\
& - [I(n'_\rho, n_\rho, |m| - 1, |m|, |m|, |m| + 1, |m|, \alpha_1^2 \rho_i^2(z)) \\
& - I(n'_\rho, n_\rho, |m| - 1, |m|, |m|, |m| + 1, |m|, \alpha_1^2 \rho_f^2(z))] \} \\
& + \frac{1}{2} [G(n'_\rho, n_\rho, |m| - 1, |m|, \alpha_1^2 \rho_i^2(z)) - G(n'_\rho, n_\rho, |m| - 1, |m|, \alpha_1^2 \rho_f^2(z))] \\
& \cdot \langle n'_z | z - z_3 | n_z \rangle_{z_i}^{z_f} \} \quad , m < 0
\end{aligned} \tag{119}$$

$$\begin{aligned}
& \langle n'_\rho m' n'_z | \{ \mathbf{\Omega}^+(v_{g1}), [\theta(z - z_i) - \theta(z - z_f)] [\theta(\rho - \rho_i(z)) - \theta(\rho - \rho_f(z))] \} | n_\rho m n_z \rangle = \\
& \delta_{m'm+1} m_0 \omega_g^2 \left\{ [I(n'_\rho, n_\rho, |m| + 1, |m|, |m| + 2, |m| + 1, |m| + 1, \alpha_1^2 \rho_i^2(z)) \right. \\
& - I(n'_\rho, n_\rho, |m| + 1, |m|, |m| + 2, |m| + 1, |m| + 1, \alpha_1^2 \rho_f^2(z))] \\
& \cdot \left\{ \frac{1}{\alpha_1} \left[2 \left\langle n'_z \left| \frac{\partial}{\partial z} \right| n_z \right\rangle_{z_i}^{z_f} + \langle n'_z | n_z \rangle (z = z_i) - \langle n'_z | n_z \rangle (z = z_f) \right] \right. \\
& \left. - 2 \alpha \langle n'_z | z - z_3 | n_z \rangle_{z_i}^{z_f} \right\} \\
& - \rho_3 [I(n'_\rho, n_\rho, |m| + 1, |m|, |m| + 2, |m| + 1, |m| + \frac{1}{2}, \alpha_1^2 \rho_i^2(z)) \\
& - I(n'_\rho, n_\rho, |m| + 1, |m|, |m| + 2, |m| + 1, |m| + \frac{1}{2}, \alpha_1^2 \rho_f^2(z))] \\
& \cdot \left[2 \left\langle n'_z \left| \frac{\partial}{\partial z} \right| n_z \right\rangle_{z_i}^{z_f} + \langle n'_z | n_z \rangle (z = z_i) - \langle n'_z | n_z \rangle (z = z_f) \right] \\
& + 2 \{ 2 \alpha_1 [I(n'_\rho, n_\rho, |m| + 1, |m| + 1, |m| + 2, |m| + 1, |m| + 1, \alpha_1^2 \rho_i^2(z)) \\
& - I(n'_\rho, n_\rho, |m| + 1, |m| + 1, |m| + 2, |m| + 1, |m| + 1, \alpha_1^2 \rho_f^2(z))] \\
& - \frac{1}{2} [G(n'_\rho, n_\rho, |m| + 1, |m|, \alpha_1^2 \rho_i^2(z)) - G(n'_\rho, n_\rho, |m| + 1, |m|, \alpha_1^2 \rho_f^2(z))] \} \\
& \cdot \langle n'_z | z - z_3 | n_z \rangle_{z_i}^{z_f} \} \quad , m \geq 0
\end{aligned} \tag{120}$$

$$\begin{aligned}
& \langle n'_\rho m' n'_z | \{ \mathbf{\Omega}_z(v_{g1}), [\theta(z - z_i) - \theta(z - z_f)] [\theta(\rho - \rho_i(z)) - \theta(\rho - \rho_f(z))] \} | n_\rho m n_z \rangle = \\
& m_0 \omega_g^2 m \delta_{m'm} \{ [I(n'_\rho, n_\rho, |m|, |m|, |m| + 1, |m| + 1, |m|, \alpha_1^2 \rho_i^2(z)) \\
& - I(n'_\rho, n_\rho, |m|, |m|, |m| + 1, |m| + 1, |m|, \alpha_1^2 \rho_f^2(z))] \\
& - \rho_3 \alpha_1 [I(n'_\rho, n_\rho, |m|, |m|, |m| + 1, |m| + 1, |m| - \frac{1}{2}, \alpha_1^2 \rho_i^2(z)) \\
& - I(n'_\rho, n_\rho, |m|, |m|, |m| + 1, |m| + 1, |m| - \frac{1}{2}, \alpha_1^2 \rho_f^2(z))] \}
\end{aligned} \tag{121}$$

* rgberg@ifin.nipne.ro

- [1] E. Merzbacher, *Quantum Mechanics* (John Wiley and Sons Inc., New York, 1961).
- [2] J. Maruhn and W. Greiner, Z. Phys. **251**, 431 (1972).
- [3] W. vonOertzen, Z. Phys. **354** 1, 37 (1996).
- [4] A. Thiel, J. Phys. G: Nucl. Part. Phys. **16**, 867 (1990).
- [5] J. W. Park, W. Scheid and W. Greiner, Phys. Rev. **C21**, 958 (1980).
- [6] D. N. Poenaru, M. Ivascu and W. Greiner, *Fission and Beta-Delayed Decay Modes*, vol. III, (CRC Press, Boca Raton, Florida, (1989); D. N. Poenaru and W. Greiner, *Nuclear Decay Modes* (Institute of Physics Publishing, Bristol, England, ch.6, (1996))
- [7] R. A. Gherghescu, J. Skalski, Z. Patyk and A. Sobiczewski, Nucl. Phys. **A651**, 237 (1999).
- [8] W. I. van Rij and C. T. Hess, Nucl. Phys. **A142**, 72 (1970).
- [9] E. Badraxe, M. Rizea and A. Sandulescu, Rev. Roum. Phys. **19**, 63 (1974).
- [10] P. Moeller, J. R. Nix and K.-L. Kratz, Atomic Data Nucl. Data Tables **66**, 131, (1997).
- [11] A. C. Wahl, Atomic Data Nucl. Data Tables, **39**, 1, (1998).

FIGURE CAPTIONS

Figure 1 Nuclear shape and deformation parameters for necked-in intersected ellipsoids. O_1 , O_2 and O_3 are the centers of the two deformed fragments and of the neck sphere respectively. The four geometrical parameters which vary are the two ratios of the ellipsoid semiaxes, b_1/a_1 and b_2/a_2 , the neck sphere radius R_3 and the distance between the fragment centers R .

Figure 2 Sequences of shapes when geometrical parameters are varied. Neck sphere radius vary from small (upper row - close to fusion shapes) through intermediary (second and third row) up to large values for very elongated shapes. Along one row, the distance between centers is increased for the same value of the neck. Semiaxes ratios and mass asymmetry here are kept constant.

Figure 3 Matching potential ellipsoids: MPE between the two fragments (shaded area) and between the neck potential and the fragment potentials (grey area). The influence of each of the potentials is emphasized in the upper part. The same figure with the surface functions for the regions of interest (fragments: $\rho_1(z)$ and $\rho_2(z)$; neck: $\rho_g(z)$; MPE: $\rho(z)$; MPE1: $\rho_{m1j}(z)$, $\rho_{m1s}(z)$, MPE2: $\rho_{m2s}(z)$ and $\rho_{m2j}(z)$ and the z -values used in calculations are marked.

Figure 4 The evolution the two fragment potentials $V_1(\rho, z)$, $V_2(\rho, z)$ and the neck potential $V_g(\rho, z)$ for the ρ -value at the two tangent points of the neck with the fragment ellipsoids: $\rho(z_{c1})$ - upper figure and $\rho(z_{c2})$ when the distance between centers increases. One can observe how the three potentials are tangent all along the splitting.

Figure 5 Variation of the heavy fragment potential $V_1(\rho, z)$ and neck potential $V_g(\rho, z)$ along the O_1O_3 direction. One can observe that inside the neck sphere - hence inside MPE1 and MPE2, the neck potential is higher, acting as a pressure element on the nuclear shape. The two crossing points at $2R_3$ distance on O_1O_3 direction mark the limits of MPE1 along the O_1O_3 direction.

Figure 6 Shell corrections calculated for the levels presented in Fig. 6, as a function of the distance between centers R . The ground state is practically common. A first bump appears in all cases; then for larger R_3 there is a decrease around $R=10$ fm. The second bump, which usually generates a second maximum in the fission barrier, lies around 15 fm, but is lower for small R_3 .

Figure 7 Two level spectra with different mass asymmetry from the same superheavy parent $^{306}122$ are presented on the upper part, for $R_3=4$ fm. The lower part of the figure shows the corresponding shell correction energy E_{shell} as a function of R . First bump is present in both cases, eventhough a little shifted. At the end of the splitting, asymmetric channel seems more favorable from microscopic point of view, as shell correction energy is some 4 MeV lower.

Figure 8 The level schemes for two fission channels from ^{252}Cf are displayed in the upper part of the figure. Levels are almost likely in the first part of the splitting as can be deduced from the corresponding shell corrections. When the two fragments continue to split, the individual wells influence results in a rather large difference in shell corrections, beyond $R=7$ fm.

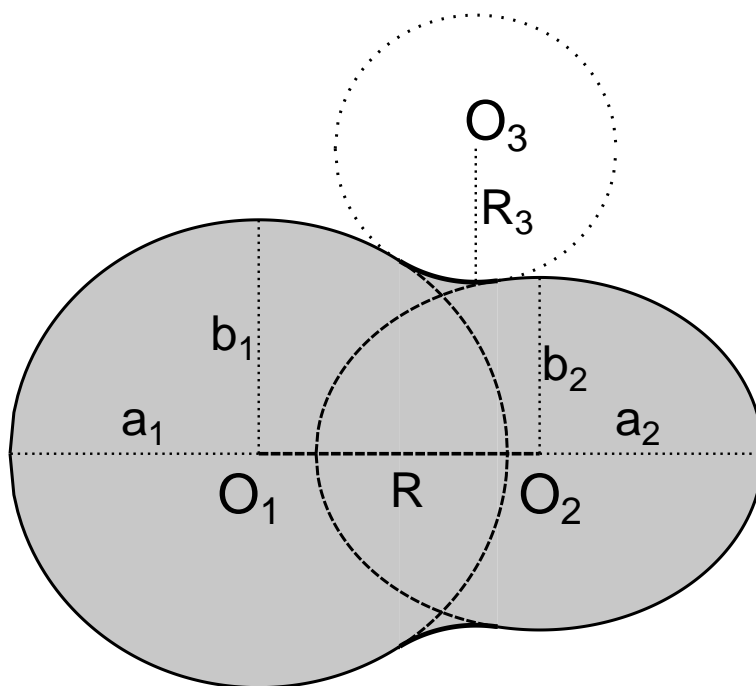


Figure 1

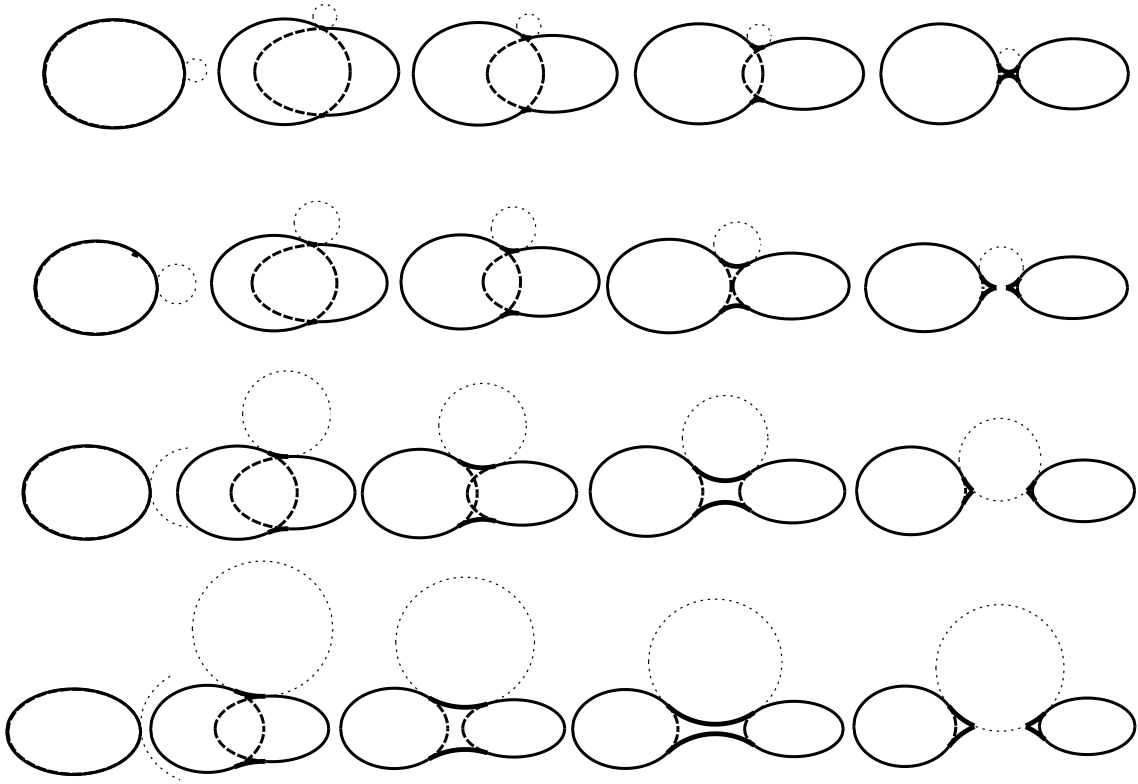


Figure 2

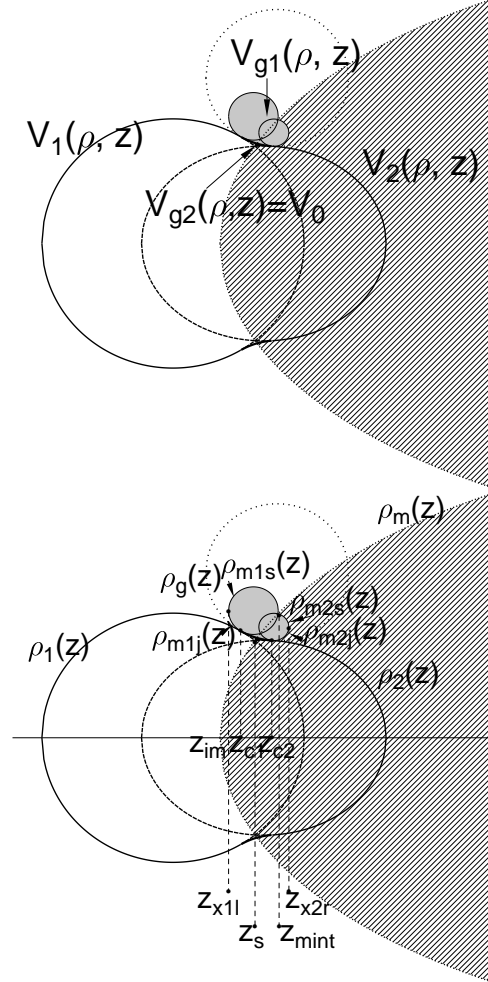


Figure 3

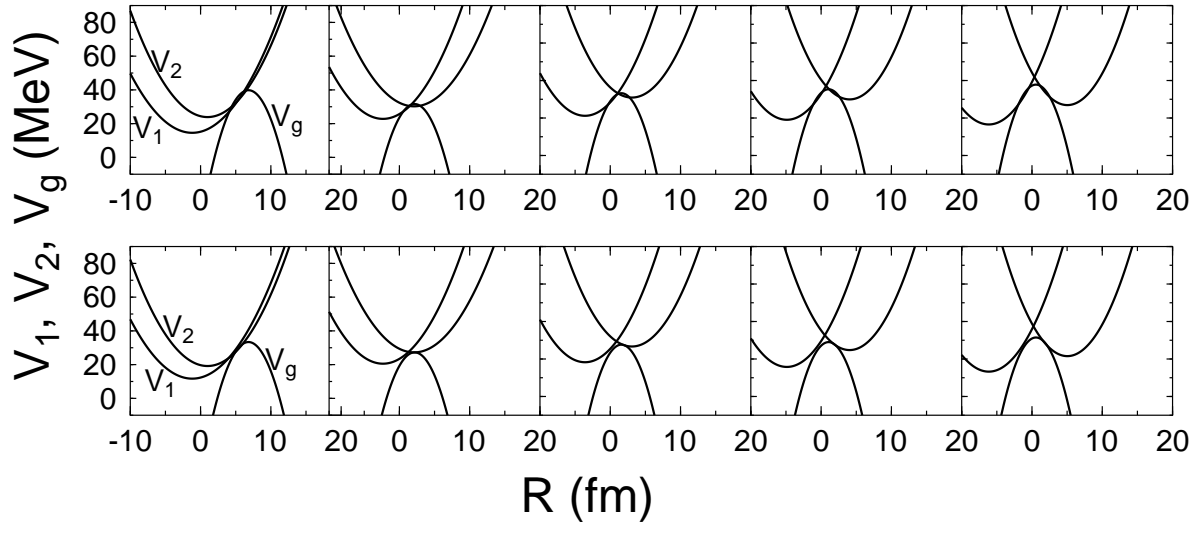


Figure 4

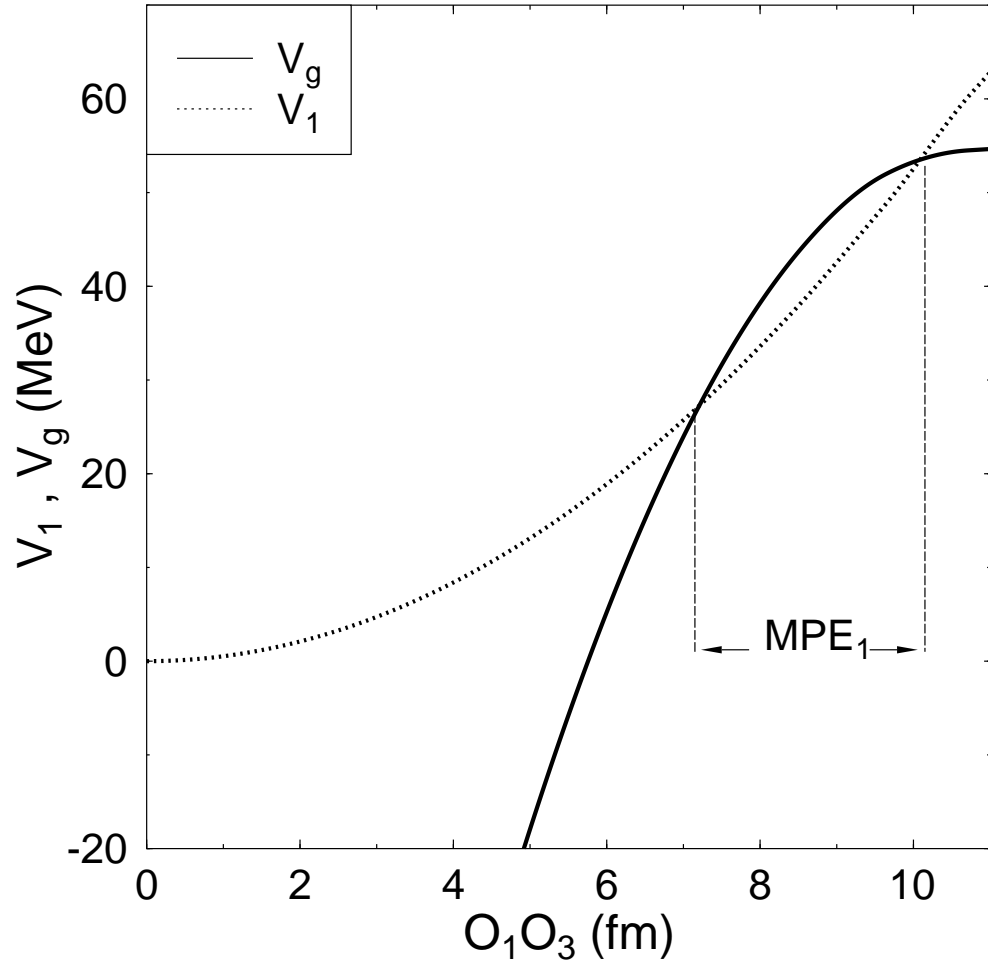


Figure 5

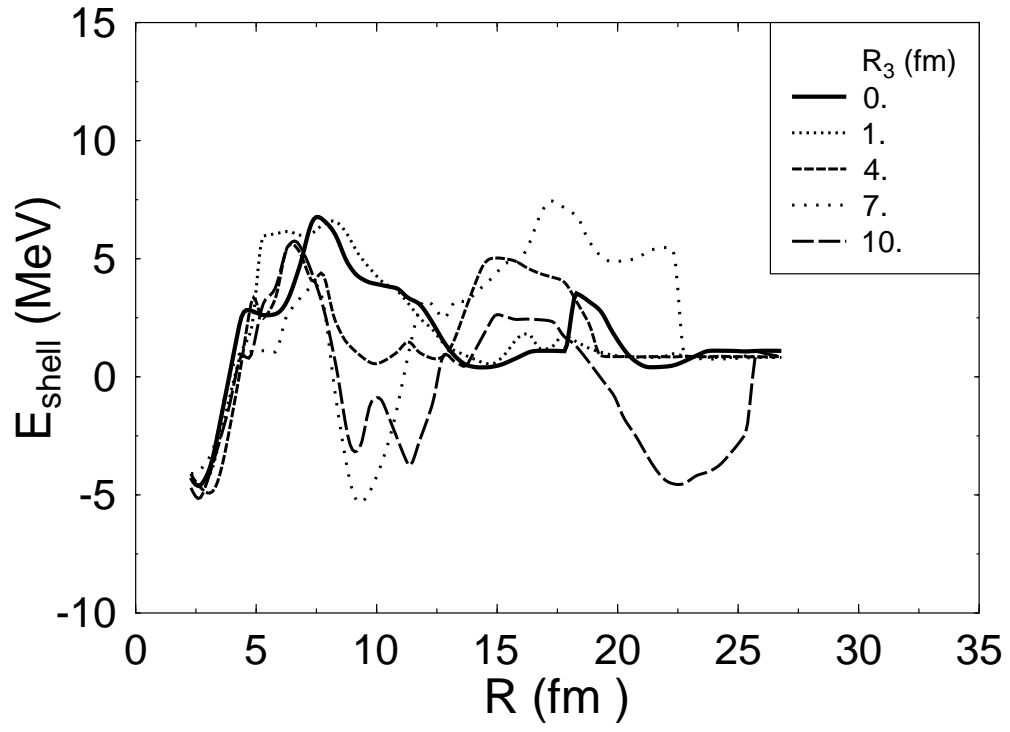


Figure 6

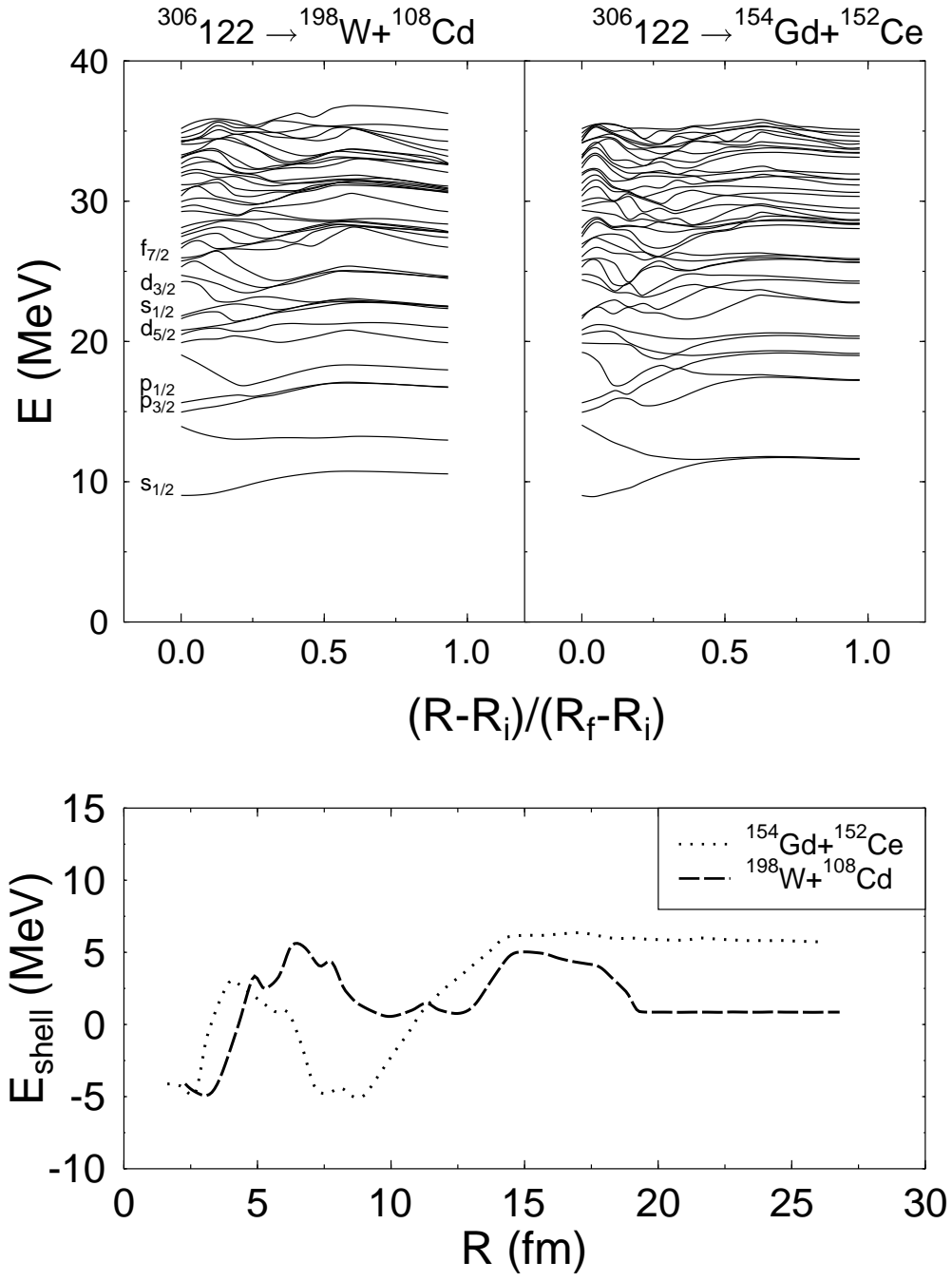


Figure 7

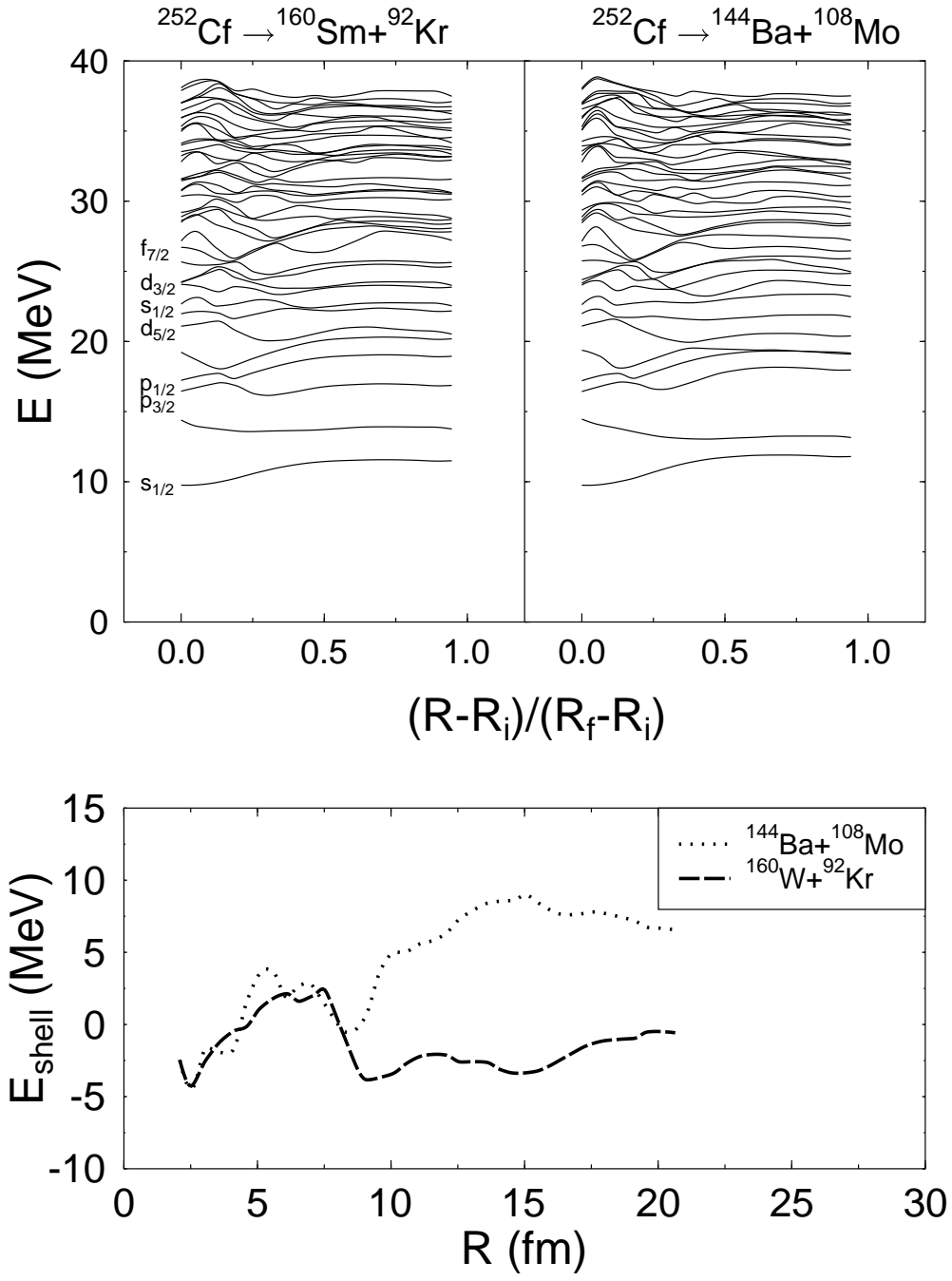


Figure 8